

# 1 Heterogeneous future Arctic Ocean primary productivity changes 2 projected in CMIP6

3 Léna Champiot-Bayard<sup>1</sup>, Lester Kwiatkowski<sup>1</sup>, Martin Vancoppenolle<sup>1</sup>

4 <sup>1</sup> LOCEAN Laboratory, Sorbonne Université-CNRS-IRD-MNHN, Paris, 75005, France

5 Correspondence to: Léna Champiot-Bayard ([lana.champiot-bayard@locean.ipsl.fr](mailto:lana.champiot-bayard@locean.ipsl.fr))

## 6 Abstract.

7 The Arctic Ocean is experiencing profound environmental changes due to climate change, with Net Primary Production  
8 (NPP) broadly projected to increase this century. This study analyzes NPP trends and their drivers across pan-Arctic and  
9 sub-regional scales throughout the 21st century, comparing Coupled Model Intercomparison Project Phase 6 (CMIP6) and  
10 Phase 5 (CMIP5) projections to assess how model generations differ. Using a multi-model approach, we assess projections  
11 for different Phytoplankton Functional Types (PFTs), diatoms and nanophytoplankton, and examine the role of physical  
12 and biogeochemical constraints including light, nutrient, and temperature limitations. Our results reveal that Arctic Ocean  
13 NPP increases are primarily driven by reduced sea ice cover, leading to longer ice-free seasons in the expanding seasonal  
14 ice zone. However, NPP changes exhibit pronounced spatial heterogeneity, with strong increases in Arctic inflow shelf  
15 regions, tempered by decreases in Baffin Bay and Nordic Seas. These differences are due to the varying balance between  
16 physical and biogeochemical NPP constraints across the Arctic Ocean. The multi-model mean Arctic Ocean NPP increase  
17 is four times larger in CMIP6 than in CMIP5, under comparable radiative forcing, with a three times higher uncertainty at  
18 the end of the century. This difference is attributed to higher baseline nutrient levels in CMIP6, combined with more  
19 pronounced sea ice loss and greater warming than in CMIP5. Key aspects to better simulate future Arctic Ocean NPP  
20 remain the representation of present-day nutrient levels, light transmission through sea ice and reduced model uncertainty  
21 in climate sensitivity.

## 22 1 Introduction

23 Phytoplankton are marine microorganisms that serve as primary producers in ocean ecosystems, forming the foundation of  
24 marine food webs (Vincent & Laybourn-Parry, 2008). Their development depends on biomass accumulation and growth  
25 rates, which are controlled by environmental factors such as light availability, nutrient concentrations and temperature.  
26 Marine Net Primary Production (NPP) represents a fundamental indicator of phytoplankton activity, quantifying net carbon  
27 fixation after losses due to cellular respiration and maintenance processes are accounted for. As an indicator of primary  
28 producer activity, NPP drives the biological ocean carbon pump and therefore plays a key role in long-term ocean carbon  
29 sequestration (Sarmiento, 2013).

30 The dependence of NPP on environmental conditions makes it sensitive to climate change. Global NPP has declined by -  
31 2.1% per decade from 1998 to 2015 according to satellite observations (Gregg & Rousseaux, 2019). Model hindcast  
32 simulations indicate NPP has declined by -6.5% since 196) and is projected to continue to decline throughout the 21<sup>st</sup>  
33 century (Bopp et al., 2013). This decrease is particularly apparent in tropical and mid-latitude regions where vertical mixing

1 [and nutrient supply decline due to enhanced upper-ocean stratification \(Doney, 2006\). In contrast, at high latitudes, and in](#)  
2 [particular in the Arctic Ocean where NPP is primarily light limited, observations suggest a recent increase in NPP, rising](#)  
3 [by 57% between 1998 and 2018 \(Lewis et al., 2020\). However, there is disagreement on the sign of the projected changes](#)  
4 [in these regions \(Laufkötter et al., 2015\).](#)

5 [The Arctic Ocean is particularly sensitive to the effects of climate change \(Kwiatkowski et al., 2020; Laufkötter et al.,](#)  
6 [2015; Vancoppenolle et al., 2013\) and is projected to experience warming nearly four times the global average \(Rantanen](#)  
7 [et al., 2022\). This warming results in ocean freshening through increased freshwater input from multiple sources, including](#)  
8 [melting glaciers and sea ice, enhanced precipitation, and greater river inflow \(McCrystall et al., 2021; Shu et al., 2018\).](#)  
9 [Moreover, climate change also impacts global ocean circulation patterns such as the Atlantic Meridional Overturning](#)  
10 [Circulation \(AMOC\), which is an important regulator of the climate system, and which could in turn have an impact on the](#)  
11 [Arctic Ocean and thus on NPP \(Weijer et al., 2020\). In polar regions, stratification is primarily driven by salinity gradients](#)  
12 [rather than temperature differences, making this freshening particularly impactful for ocean mixing and circulation patterns](#)  
13 [\(Timmermans & Marshall, 2020\).](#)

14 [The Arctic Ocean phytoplankton community consists of diatoms and smaller taxa including coccolithophores,](#)  
15 [prymnesiophytes, flagellates, and picoeukaryotes \(Ardyna & Arrigo, 2020\). Climate change is projected to drive a](#)  
16 [compositional shift toward smaller phytoplankton \(Bopp et al., 2005\), fundamentally altering marine food web structure](#)  
17 [and efficiency. This size-structure transition extends food chain length and reduces trophic transfer efficiency, consequently](#)  
18 [reducing carbon export. The shift particularly weakens export through two mechanisms: smaller phytoplankton are more](#)  
19 [efficiently recycled within the microbial loop, while larger phytoplankton like diatoms contribute disproportionately to](#)  
20 [carbon export via gravitational sinking. These structural modifications have cascading effects on both ecosystem](#)  
21 [functioning and carbon sequestration capacity \(Grebmeier et al., 2010; Ward et al., 2012\). Furthermore, phytoplankton](#)  
22 [community restructuring propagates through upper trophic levels, ultimately impacting commercial fisheries and marine](#)  
23 [food security \(Ardyna & Arrigo, 2020; Hegseth & Sundfjord, 2008; Neukermans et al., 2018\). The implications of global](#)  
24 [warming on the Arctic Ocean extend beyond primary productivity and encompass Arctic Ocean biogeochemical cycles,](#)  
25 [especially the carbon pump and the regional contribution to climate regulation \(Sarmiento, 2013\).](#)

26 [Arctic Ocean NPP has increased by >50% over recent decades, according to satellite observations \(Arrigo & van Dijken,](#)  
27 [2015; Lewis et al., 2020\). This increase is largely attributed to the decrease in sea ice coverage and thickness, as well as](#)  
28 [associated changes in sea ice scape, which enhances light penetration into the water column and fosters higher](#)  
29 [phytoplankton productivity \(Lannuzel et al., 2020\). Additionally, riverine fluxes and coastal erosion supply a substantial](#)  
30 [amount of nutrients, supporting approximately one-third of Arctic Ocean productivity \(Terhaar et al., 2021\).](#)

31 [The Arctic Ocean is projected to experience a continued increase in NPP under climate change \(Tagliabue et al., 2021\).](#)  
32 [Future sea ice retreat will further extend the open-water season duration, enhance light availability and stimulate](#)  
33 [phytoplankton growth. However, the melting of sea ice will also introduce large volumes of freshwater, which may further](#)  
34 [stratify the water column, reducing nutrient transport from deeper waters and potentially modifying NPP dynamics \(Pabi](#)  
35 [et al., 2008; Popova et al., 2010\) and the distribution of the phytoplankton in the water column \(Steiner et al., 2016\).](#)

36 [CMIP5 Arctic Ocean NPP projections exhibited considerable model divergence with even the sign of future Arctic Ocean](#)  
37 [NPP anomalies uncertain \(Vancoppenolle et al., 2013\). However, there is model agreement on the driving mechanisms:](#)  
38 [decreasing sea ice extent \(and thus increasing light availability\) and declining nitrate concentrations, almost reaching an](#)

1 [oligotrophy onset in 2100. Increased temperatures could also contribute to enhanced NPP, however the analysis of CMIP5](#)  
2 [projections did not consider thermal sensitivity as a mechanism influencing NPP \(Vancoppenolle et al., 2013\). There is](#)  
3 [also a high uncertainty amongst CMIP5 models concerning the deepening of the future Subsurface Chlorophyll Maximum](#)  
4 [\(SCM\) \(Steiner et al., 2016\).](#)

5 Despite the recognized importance of environmental drivers in controlling Arctic phytoplankton productivity, several  
6 critical knowledge gaps remain. First, it is unclear how projections of key environmental factors (light availability, nutrient  
7 concentrations, and temperature) have evolved between CMIP5 and CMIP6 model generations, and whether improved  
8 model physics in CMIP6 has led to more consistent or divergent projections. Second, the relative importance of these  
9 drivers in CMIP6 varies spatially across the Arctic Ocean, but a systematic analysis of these spatial patterns is lacking.  
10 Third, different PFTs respond differently to environmental changes, yet how these differential responses are captured across  
11 regions remains poorly understood. Finally, while previous studies have identified sign inconsistencies in CMIP5 NPP  
12 projections (Vancoppenolle et al., 2013), the mechanisms underlying the substantially larger NPP increases projected by  
13 CMIP6 models have not been systematically analyzed in the Arctic Ocean (Tagliabue et al., 2021). These gaps limit our  
14 ability to assess the reliability of future Arctic Ocean productivity projections and their implications for marine ecosystems  
15 and biogeochemical cycles.

a supprimé: (Vancoppenolle et al., 2013)

a supprimé: (Tagliabue et al., 2021)

16 To address this knowledge gap, we investigate the environmental drivers of phytoplankton growth using both CMIP6 and  
17 CMIP5 models. Our analysis aims to understand how projections and associated uncertainties have changed between the  
18 two model generations over the 21st century, examine spatial variations in these projections across the Arctic Ocean, and  
19 assess how different phytoplankton functional types respond to these environmental changes.

## 20 **2 Material and Methods**

### 21 **2.1 Model selection**

22 We used output from the Coupled Model Intercomparison Project Phase 6 (Eyring et al., 2016) downloaded from the Earth  
23 System Grid Federation (ESGF) servers (Table 1). Each ESM member is identified by a nomenclature composed of letters  
24 and various numbers, such as *rWiXpYZ*, where *W* indicates the realization number (different for each run), *X* denotes the  
25 initialization method, *Y* refers to the set of physical parameterizations used, and *Z* represents the forcing configuration  
26 number. For each model, we prioritized selecting the ensemble member r1i1p1f1 when available. If r1i1p1f1 was not  
27 available, the ensemble member most similar to it, such as r2i1p1f1, r1i1p1f2, or the closest alternative was chosen. The  
28 historical period spans 1850-2014, while the SSP scenarios cover 2015-2100. Five SSP scenarios were selected: SSP1-2.6,  
29 SSP2-4.5, SSP3-7.0, SSP5-3.4 and SSP5-8.5 (Meinshausen et al., 2020).

a supprimé: (Eyring et al., 2016)

a supprimé: where

Code de champ modifié

30 To compare with the previous generation of models, from the Coupled Model Intercomparison Project Phase 5 (Taylor et  
31 al., 2012), we downloaded output from ESGF servers (Table 2) for the scenario RCP8.5 (van Vuuren et al., 2011). As with  
32 CMIP6, we prioritized r1i1f1 when possible. The CMIP5 historical period spans from 1850 to 2005 while the RCP8.5  
33 scenario covers the period 2006-2100.

a supprimé: (Taylor et al., 2012)

a supprimé: only

a supprimé: (Riahi et al., 2011)

34 Although additional scenarios were briefly examined, the detailed analysis is restricted to SSP5-8.5 and RCP8.5 (as in  
35 Vancoppenolle et al., 2013), since the primary objective of this study is to investigate the dominant mechanisms and  
36 processes underlying future changes rather than to provide precise scenario-dependent projections.

1

## 2 2.2 Models diagnostic

### 3 2.2.1 Study region and interpolation methods

4 The Arctic Ocean was defined as the waters above 66.5°N latitude and divided into 10 different regions, following (Arrigo  
5 & van Dijken, 2011). Both model output and observations were interpolated onto a regular latitude-longitude grid with a  
6 resolution of 360×180 using the CDO (Climate Data Operators) software with the remapdis interpolation method  
7 (Schulzweida, 2023).

### 8 2.2.2 NPP diagnostics

9 Model outputs are not always available for all variables of interest, so we categorized the models into two groups based on  
10 data availability (Table 1), corresponding to the two sections of our study: In the first section, we examined the prognostic  
11 environmental variables that may influence NPP, namely NO<sub>3</sub> concentrations, sea ice concentrations and sea surface  
12 temperatures (respectively named in CMIP6: no3, sic and tos) and in the second section we investigated the light, nutrient  
13 and thermal limitation terms that directly impact phytoplankton growth rates. The first section uses outputs from Group 1  
14 and Group 2 models, while the second section focuses on models from Group 2, which provide direct limitation term  
15 diagnostics. These limitation terms are derived from the variables mentioned above and represent key factors influencing  
16 phytoplankton growth rate (μ) for a given phytoplankton type:

$$\mu = \mu_{max} \times T_f \times L_{lim} \times N_{lim} \quad (1)$$

17 where  $\mu_{max}$  is the maximum growth rate,  $L_{lim}$  and  $N_{lim}$  are the limitation terms for light and nutrient respectively, and  $T_f$   
18 represents the temperature function.

### 19 2.2.3 Nutrients, SST, Sea ice and limitation factors

20 Nitrate (NO<sub>3</sub>) was selected as the limiting nutrient, as the Arctic Ocean is primarily nitrogen-limited, and ammonium (NH<sub>4</sub>)  
21 is not available for all models (Browning & Moore, 2023; Tremblay & Gagnon, 2009). Two different approaches were  
22 used to calculate nitrate concentrations. When data were available, nitrate concentrations were integrated over the mixed  
23 layer (MLD). However, as mixed-layer depth and vertically-resolved NO<sub>3</sub> data were not available for all scenarios  
24 (especially for CMIP5), some analyses were conducted using surface nitrate concentrations, i.e., from the upperocean  
25 model layer. An oligotrophy threshold was set at 1.6 mmol/m<sup>3</sup>, i.e., at the half-saturation constant of diatoms for NO<sub>3</sub>  
26 uptake (Sarhou et al., 2005). Additional analysis is provided in the appendix, where NO<sub>3</sub> is integrated over the upper 100m  
27 of the water column (see Fig. A1).

28 As a diagnostic of ice coverage, we used monthly mean sea ice concentration (SIC) outputs. From this, we derived  
29 the September sea ice area (SSIA), the mean September sea ice concentration (SSIC), and the mean ice-free season duration  
30 (IFSD). The IFSD was defined as the number of months with sea ice concentration lower than 15% (Lebrun et al., 2019).

31 We analyzed growth rates for the two PFTs available in model output: diatoms and miscellaneous phytoplankton. The  
32 direct limitation terms provided by the models include: the light limitation term for miscellaneous phytoplankton ( $L_{lim}^{misc}$ ,  
33 named limirmisc in CMIP6 terminology), the light limitation term for diatoms ( $L_{lim}^{diat}$ , limirrdiat), the nutrient limitation  
34 term for miscellaneous phytoplankton ( $N_{lim}^{misc}$ , limnmisc) and the nutrient limitation term for diatoms ( $N_{lim}^{diat}$ , limndiat).

a supprimé: The Arctic Ocean was defined as the waters above 66.5°N latitude and divided into 10 different regions, following (Arrigo & van Dijken, 2011). Both model output and observations were interpolated onto a regular latitude-longitude grid with a resolution of 360×180 using the CDO (Climate Data Operators) software with the remapdis interpolation method (Schulzweida, 2023).  
2.2.2 NPP diagnostics

a supprimé: parts

a supprimé: a

a supprimé: part

a supprimé: part

a supprimé: This

a supprimé: part of study used

a supprimé: . The

a supprimé: part of our study

a supprimé: (1)

a supprimé: Nitrate (NO<sub>3</sub>) was selected as the limiting nutrient, as the Arctic Ocean is primarily nitrogen-limited, and ammonium (NH<sub>4</sub>) is not available for all models (Browning & Moore, 2023; Tremblay & Gagnon, 2009). Two different approaches were used to estimate nitrate concentrations. When data were available, nitrate concentrations were integrated over the mixed layer (MLD). However, as mixed-layer depth (MLD) and vertically-resolved NO<sub>3</sub> data were not available for all scenarios (especially for CMIP5), some analyses were conducted using surface nitrate concentrations, i.e., from the first vertical ocean model layer. An oligotrophy threshold was set at 1.6 mmol/m<sup>3</sup>, i.e., at the half-saturation constant of diatoms for NO<sub>3</sub> uptake (Sarhou et al., 2005). An additional figure in the appendix are shown, where NO<sub>3</sub> is integrated in the first 100m of the water column (see Fig. A1).  
As a diagnostic of ice coverage, we used monthly mean sea ice concentration (SIC) outputs. From the latter, we derived the September sea ice area (SSIA), the mean September sea ice concentration (SSIC), and the mean ice-free season duration (IFSD). The IFSD was defined as the number of months with sea ice concentration lower than 15% (Lebrun et al., 2019).  
We analyzed growth rates for the two PFTs available in these models

1 These limitation terms can vary between 0 and 1, with lower values indicative of greater constraint on phytoplankton  
 2 growth rates.  
 3 The temperature function ( $T_f$ ) is not directly provided by the models, but it is calculated using the Eppley function ( $\mu_{max} =$   
 4  $0.59e^{0.0633T}$ , where  $K_{Eppley} = 0.063^\circ\text{C}^{-1}$ ). except for UKESM1-0-LL which calculates the temperature function as  $T_f = 1.006^T$ ,  
 5 based on vertically gridded **potential** temperature (3Dtemp, thetao). Monthly  $T_f$  was computed for each depth level and  
 6 weighted according to the biomass of each PFT (phymisc or phydiat) to obtain PFT-specific depth integrated temperature  
 7 functions for each model ( $T_f^{misc}$  and  $T_f^{diat}$ ).

a supprimé: differently,

a supprimé: in CMIP6 terminology

a supprimé: in CMIP6 terminology

	Model (reference)	Ocean - Sea-ice - Biogeochemical components	Available Variables	Available Simulations					
				historical	SSP1-2.6	SSP2-4.5	SSP3-7.0	SSP5-3.4	SSP5-8.5
Group 1	CESM2 (Danabasoglu et al., 2020)	POP2 - CICE5 - MARBL-BEC	NPP, NO3, SIC, SST	x	x	x	x		x
			MLD	x					x
	CESM2-WACCM (Danabasoglu, 2019)	POP2 - CICE5 - MARBL-BEC	NPP, SIC, SST	x	x	x	x	x	x
			NO3	x	x	x	x		x
	CanESM5 (Swart et al., 2019)	NEMO3.4 - LIM2 - CMOG	MLD	x					x
			NPP, NO3	x	x	x	x		x
	CanESM5-CanOE (Christian et al., 2022)	NEMO3.4 - LIM2 - CanOE	SIC, SST	x	x	x	x	x	x
			MLD	x					x
	MIROC-ES2L (Hajima et al., 2020)	COCO - OECO2	NPP, NO3, SIC, SST	x	x	x	x	x	x
	MPI-ESM1-2-HR (Mauritsen et al., 2019)	MPIOM - HAMOCC6	NPP, NO3, SIC, SST	x	x	x	x		x
			MLD	x					x
MPI-ESM1-2-LR (Mauritsen et al., 2019)	MPIOM - HAMOCC6	NPP, NO3, SIC, SST	x	x	x	x		x	
		MLD	x					x	
MRI-ESM2-0 (Yukimoto et al., 2019)	MRICOM4 - NPZD	NPP, NO3, SIC, SST	x					x	
NorESM2-LM (Tijputra et al., 2020)	BLOM - CICE5 - IHAMMOG	NPP, SIC, SST	x	x	x	x	x	x	
		NO3	x	x				x	
		MLD	x					x	
Group 2	CNRM-ESM2-1 (Séférian et al., 2019)	NEMOv3.6 - GELATOV6 - PISCESv2-gas	NPP, SIC, SST	x	x	x	x	x	x
			$L_{lim}^{diat}, L_{lim}^{misc}, N_{lim}^{diat}, N_{lim}^{misc}$ , phydiat, phymisc, 3Dtemp, MLD	x					x
			NO3	x	x	x	x		x
	GFDL-ESM4 (Dunne et al., 2020)	MOM6 - SIS2 - COBALTv2	NPP, NO3, SIC, SST	x	x	x	x		x
	NEMOv3.6 - LIM3 - PISCESv2	$L_{lim}^{diat}, L_{lim}^{misc}, N_{lim}^{diat}, N_{lim}^{misc}$ , phydiat, phymisc, 3Dtemp, MLD	x					x	
	NEMOv3.6 - LIM3 - PISCESv2	NPP, NO3, SIC, SST	x	x	x	x	x	x	

a supprimé: GFDL-ESM4 (Dunne et al 2020b ; Stock et al, 2020)...

IPSL-CM6A-LR (Boucher et al., 2020)	NEMO v3.6 - CICE - MEDUSA-2	$L_{lim}^{diat}, L_{lim}^{misc}, N_{lim}^{diat}, N_{lim}^{misc}$ , phydiat, phymisc, 3Dtemp, MLD	x						x
		NPP, SIC, SST	x	x	x	x	x	x	x
UKESM1-0-LL (Sellar et al., 2019)	NEMO v3.6 - CICE - MEDUSA-2	$L_{lim}^{diat}, L_{lim}^{misc}, N_{lim}^{diat}, N_{lim}^{misc}$ , phydiat, phymisc, 3Dtemp, MLD	x						x
		NO3	x	x	x	x			x

**Table 1:** Description of CMIP6 models used in this study, along with the associated available variables and simulations. The first group includes models used to project environmental conditions (NPP, NO<sub>3</sub>, SIC, and SST). The second group includes models used for both environmental projections and analysis of phytoplankton growth limitation terms ( $N_{lim}$ ,  $L_{lim}$  and  $Tf$ ).

a supprimé: scenario

1

Model (reference)	Ocean - Sea-ice -biogeochemical components	Available Variables	Available Simulations
<b>CESM1-BGC</b> (Moore et al., 2013)	POP - CICE4 – BEC	SST	historical, RCP8.5
<b>CMCC-CESM</b> (Fogli & Iovino, 2014)	NEMO3.4 - CICE4 – CMCC	NO3, SIC, SST	historical, RCP8.5
<b>GFDL-ESM2G</b> (Dunne et al., 2013)	ESM2G – MOM4p1 – TOPAZ2	NPP, NO3, SIC, SST	historical, RCP8.5
<b>GFDL-ESM2M</b> (Dunne et al., 2013)	ESM2M – MOM4p1 – TOPAZ2	NPP, NO3, SIC, SST	historical, RCP8.5
<b>HadGEM2-ES</b> (The HadGEM2 Development Team: G. M. Martin et al., 2011)	HadGEM2 – Diat-HadOCC	SST	historical, RCP8.5
<b>IPSL-CM5A-LR</b> (Dufresne et al., 2013)	NEMO - LIM2 - PISCES	NPP, NO3, SIC, SST	historical, RCP8.5
<b>IPSL-CM5A-MR</b> (Dufresne et al., 2013)	NEMO - LIM2 - PISCES	NPP, SIC, SST	historical, RCP8.5
<b>MIROC-ESM</b> (Watanabe et al., 2011)	COCO – NPZD-type	NPP	historical, RCP8.5
<b>MIROC-ESM-CHEM</b> (Watanabe et al., 2011)	COCO – NPZD-type	NPP	historical, RCP8.5
<b>MPI-ESM-LR</b> (Ilyina et al., 2013)	– HOMOC5.2	NPP, NO3, SIC, SST	historical, RCP8.5
<b>MPI-ESM-MR</b> (Ilyina et al., 2013)	– HOMOC5.2	NPP, SIC, SST	historical, RCP8.5
<b>NorESM1-ME</b> (Bentsen et al., 2013)	MICOM – CICE4 – HAMOC-ME	NO3, SST	historical, RCP8.5

a supprimé: CESM1-BGC (Moore et al., 2013)

2 **Table 2:** CMIP5 models used in this study, along with the available variables and simulations.

a supprimé: scenario

### 3 **2.3 Data used for model evaluation**

a supprimé: We did more individual model and regional analysis which are provided in the appendix.¶

#### 4 *Primary Production*

5 The primary production **observational data product** used in this study provides recalculated depth-integrated NPP values  
6 based on satellite-derived chlorophyll concentrations, sea surface temperature, and sea ice cover (Lewis et al., 2020). This  
7 dataset spans 1998–2018 and offers satellite-based estimates in the Arctic Ocean. It was regridded onto a  $1^\circ \times 1^\circ$  spatial  
8 resolution. Only NPP data from March 1st to September 30th were considered for model evaluation, due to the lack of  
9 ocean color observations during the dark season.

a supprimé: dataset

a supprimé: (Lewis et al., 2020)

#### 10 *Nitrate (NO<sub>3</sub>)*

11 To evaluate nitrate concentrations, we used a climatology derived from in situ hydrographic observations from the World  
12 Ocean Atlas 2018 (Garcia et al., 2019; Randelhoff et al., 2020). This dataset provides an average nitrate concentration  
13 from 1978 to 2017 on a  $1^\circ \times 1^\circ$  grid. Observed nitrate concentrations were extracted over the upper 100m of the ocean.  
14 Depending on analysis, depth-averaging was performed consistently with model output, as detailed in Section 2.2.3.  
15 However, nitrate data in the Arctic Ocean remain sparse, particularly in summer, and may be subject to significant biases  
16 (Gibson et al., 2020).

a supprimé: To evaluate nitrate concentrations we used a climatology derived from in situ hydrographic observations from the World Ocean Atlas 2018 (Garcia et al., 2019; Randelhoff et al., 2020). This dataset provides an average nitrate concentration from 1978 to 2017 on a  $1^\circ \times 1^\circ$  grid. Nitrate concentrations were extracted over the full water column, representing the upper 100 m of the ocean. However, nitrate data in the Arctic Ocean remain sparse, particularly in summer, and may be subject to significant biases (Popova et al., 2012).¶

1 *Sea ice concentration*

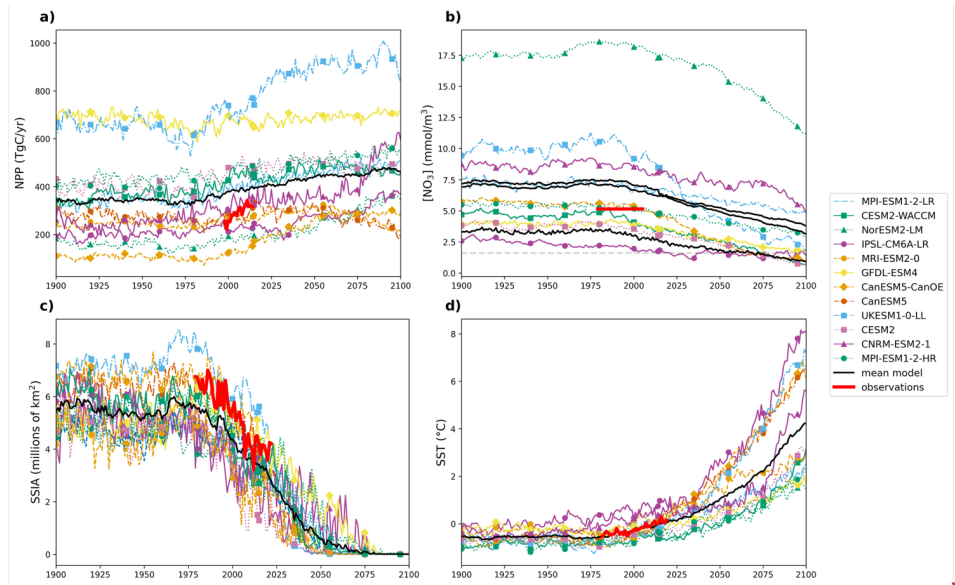
2 Passive microwave satellite sea ice concentration fields were taken from the [OSI-SAF Global sea ice concentration data](#)  
 3 [record v3 \(OSI SAF, 2022\)](#). This dataset provides daily averaged sea ice cover (in percentage) at 25 km spatial resolution,  
 4 covering the period 1979–2022.

5 *Sea Surface Temperature (SST)*

6 The sea surface temperature [observational](#) dataset is derived from the Climate Change Initiative (CCI) satellite product,  
 7 covering the period 1982–2019, providing daily analyses at a high spatial resolution of 0.05° ([Embury, O., 2024](#)). This  
 8 dataset provides a long-term, high-quality observational record of SST, allowing for comparison with model outputs.

9 **3 Results**

10 **3.1 Model evaluation**



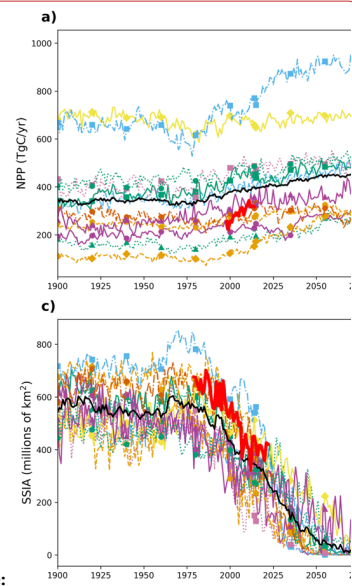
11 **Figure 1.** Projections of Arctic Ocean (a) annual mean depth-integrated NPP, (b) NO<sub>3</sub> concentration in the mixed layer depth (MLD),  
 12 (c) September Sea Ice Area (SSIA), and (d) annual mean SST, derived from individual CMIP6 models (Group 1) using historical and  
 13 SSP5-8.5 simulations over the period 1900–2100. In panel (b), three metrics are displayed as multi-model mean (black lines): the annual  
 14 maximum (February, upper line), annual mean (middle line), and annual minimum (July, lower line); individual model trajectories are  
 15 shown only for the annual mean. The horizontal grey dashed line indicates the NO<sub>3</sub> concentration threshold associated with oligotrophic  
 16 conditions. In all panels, colored lines represent individual model simulations, the thick red line represents the observations, and the  
 17 thick black line denotes the multi-model mean.

a supprimé: Global sea ice concentration data record v3 (OSI SAF, 2022).

a supprimé: a

a supprimé: 1978

a supprimé: (Embury., 2024)



a supprimé:

a supprimé: (a), February, July and annual mean NO<sub>3</sub>

a supprimé: (b),

a supprimé: (c)

a supprimé: (d)

a supprimé: group

a supprimé: ),

a supprimé: from

a supprimé: to

a supprimé: Each color represents a model, the black line is the ...

a supprimé: , and the

a supprimé: represents NO<sub>3</sub>

a supprimé: consistent with oligotrophy. The upper

a supprimé: in NO<sub>3</sub> represents

a supprimé: concentration in March, the middle one represents the annual mean concentration and the lower one represents the concentration in July

Variable	Period	Observed mean	CMIP6 mean	Observed trend (/yr)	CMIP6 trend (/yr)
NPP (TgC/yr)	1998-2018	308	389	6.73	1.30
SSIA (10 <sup>6</sup> km <sup>2</sup> )	1979-2022	5.28	4.31	-0.059	-0.056
SST (°C)	1982-2019	-0.402	-0.247	0.019	0.013

**Table 3:** Observed and simulated NPP, SSIA and SST values throughout the observational period. Nitrate concentrations are not given as an Arctic Ocean time series is not available.

Simulated ranges of NPP, MLD, NO<sub>3</sub> concentration, SSIA and SST encompass data-based estimates over the observational period (Fig. 1). While the simulated trends in Arctic Ocean warming and declining SSIA are broadly consistent with observations, simulated increases in NPP are low biased. The multi-model mean NPP is slightly higher than observed, over the 1998-2018 period over which all models consistently simulate an NPP increase. Observed NPP increases from 256 Tg C/yr in 1998 to 391 Tg C/yr in 2018, increasing by 135 Tg C/yr in 21 years. The increase in NPP in models is lower, increasing from 354 Tg C/yr to 394 Tg C/yr, increasing by 40 Tg C/yr in 21 years (Fig. 1a, Table 3). The multi-model annual mean NO<sub>3</sub> concentration for the period 1979-2005 is 6.90 mmol/m<sup>3</sup>, which is higher than the observations of 4.67 mmol/m<sup>3</sup> for the same period. However, this discrepancy is not unexpected, as Arctic Ocean NO<sub>3</sub> observations contain significant uncertainties due to limited accessibility beneath sea ice cover (Fig. 1b). Models and observations agree on a loss of sea ice coverage, although the simulated rate of decrease is lower than observed (Fig. 1c, Table 3), confirming previous studies (Notz & Community, 2020). Similarly, observed Arctic Ocean warming is ~50% higher than that simulated over the same period (Fig. 1d, Table 3).

The drivers of these projected anomalies are changing in the same direction across all Arctic subregions: NO<sub>3</sub> and September sea ice decrease and SST increases for all models and regions, consistent with earlier CMIP-based assessments (Vancoppenolle et al., 2013) (see Fig.A1, A2, A3, A4).

Several additional figures on individual model and regional analysis are provided in the appendix.

a supprimé ;

a supprimé ;

a supprimé ;

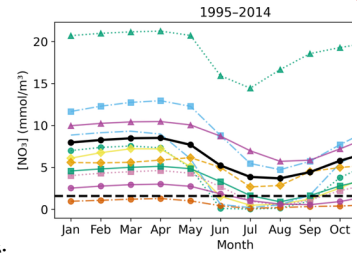
a supprimé: upper-100m

a supprimé: in 21 years

a supprimé: 40Tg

a supprimé: nutrient

a supprimé: modeled rate of decrease is lower than observed (Fig. 1c), with sea ice retreat proceeding faster in observations than simulated (Table 3), confirming previous studies (Notz & Community, 2020)

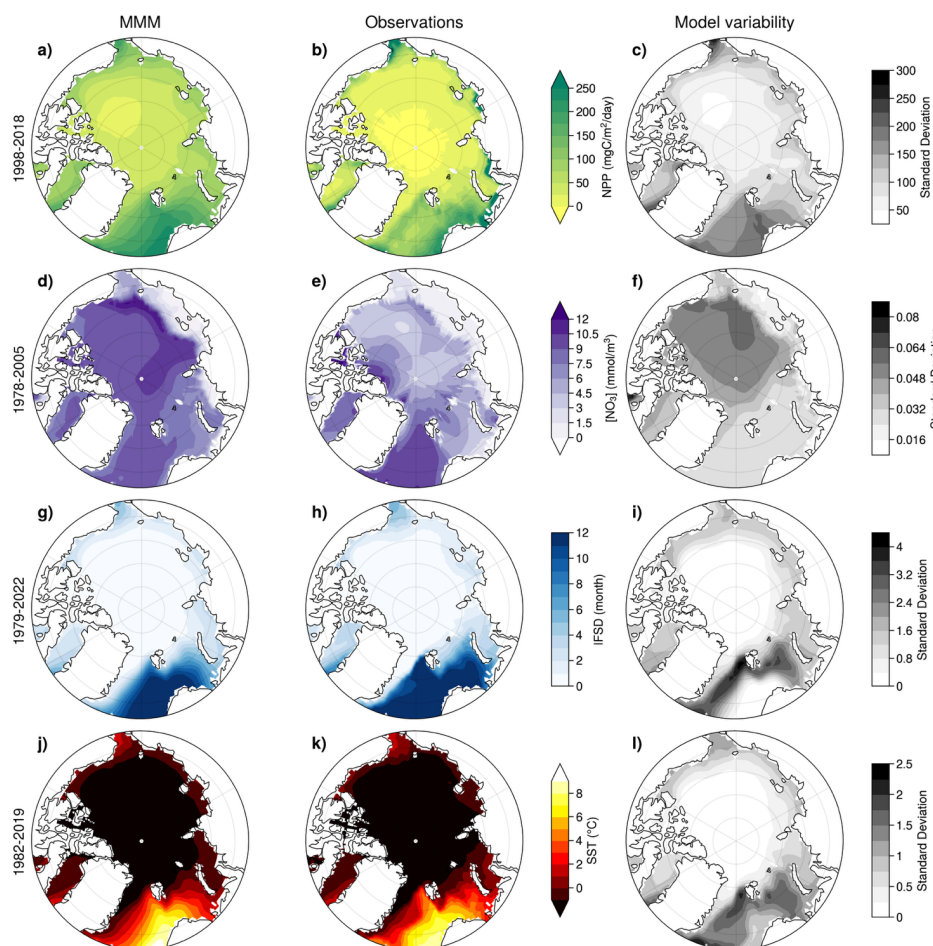


a supprimé:

**Fig 2:** Seasonal cycle of nitrate concentration during the two last decades of the historical simulation (1995-2014) (left) and the last two decades of SSP5-8.5 (2081-2100) (right). Each model is represented in a different color while the multi-model mean is shown in black.

By the end of the century, most CMIP6 models simulate a transition toward oligotrophic conditions, with an increasing fraction of ensemble members exhibiting oligotrophy and a longer seasonal persistence of these conditions (Fig. 2). The seasonal cycle of nutrient concentration indicates that during the period 1995-2014, only seven CMIP6 models reach oligotrophy during the productive period, generally from mid-May to September (CanESM5, MPI-ESM1-2-LR, MPI-ESM1-2-HR, GFDL-ESM4, CESM2, CESM2-WACCM, and IPSL-CM6A-LR). An exception occurs for IPSL-CM6A-LR, which remains oligotrophic until November, and for CanESM5, which is oligotrophic throughout the year. By the end of the century, nine models reach oligotrophy (all except MPI-ESM1-2-HR and CNRM-ESM2-1), over a longer period extending from early May to February. However, the multi-model mean is influenced by models with higher nutrient concentrations and reaches oligotrophy only during July and August.

... [1]



1  
2 **Figure 2.** NPP, NO<sub>3</sub> (integrated over the upper 100 m of the water column), IFSD, and SST, over the recent past, **as represented by the**  
3 **multi-model mean (left), observational data products (middle) and the multi-model standard deviation (right).** The averaging period  
4 corresponds to the availability of observations prior to 2015. Model outputs are combined from historical simulations for years prior to  
5 2015 and SSP5-8.5 thereafter. For NPP, the March to September average is shown.

6 The spatial distribution of key variables across the Arctic Ocean is generally well represented by the multi-model mean  
7 and comparable to **observations** despite some regional discrepancies that reflect both model limitations and observational  
8 uncertainties (Fig. 2).

9 **March-September NPP** resembles satellite-derived estimates, with the highest values in the Nordic Seas, the Bering Strait,  
10 and along the Siberian shelf, while the Arctic Basin exhibits the lowest NPP values (Fig. 2a and b). The multi-model mean  
11 IFSD and SST spatial distributions also closely **align** with observations. The warmest regions (Nordic Seas, Barents Sea,  
12 and Chukchi Sea) correspond to areas with the least sea ice (Fig. 2g, h, j and k). While the multi-model mean represents

- a supprimé: according to
- a supprimé: ) and
- a supprimé: references
- a supprimé: between models
- a supprimé: observational references
- a supprimé: 4
- a supprimé: Drivers are projected to change in the same direction across all Arctic regions : NO<sub>3</sub> and September sea ice decrease and SST increases for all models and regions, providing a continuity with earlier CMIP-based assessments (Vancoppenolle et al., 2013) (see Fig.A1, A2, A3, A4).¶
- ...
- a supprimé: 4a
- a supprimé: aligns
- a supprimé: 4g

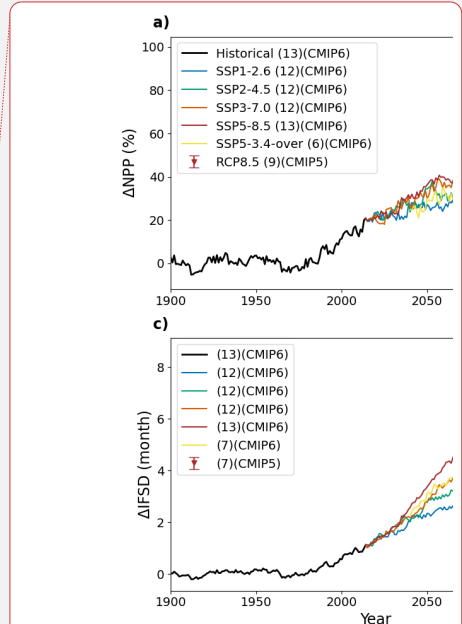
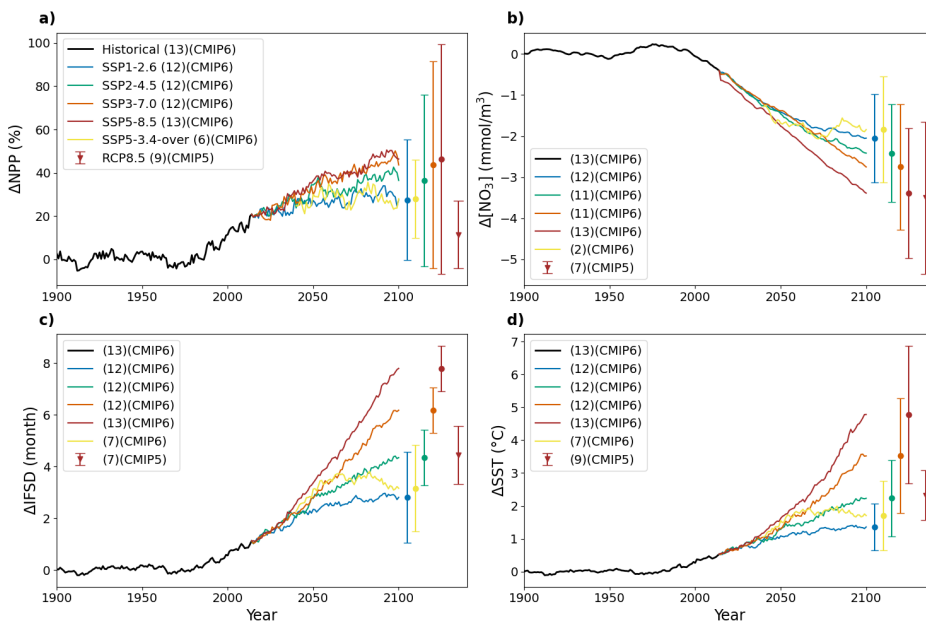
low values for coastal NO<sub>3</sub> concentrations, in the Chukchi Sea and along the eastern Arctic Basin, it may overestimate nitrate concentrations in the Arctic Basin, though observations in this region remain limited. The coastal shelves of the Kara, Laptev and East Siberian Seas show low NO<sub>3</sub> values — of less than 1.5 mmol/m<sup>3</sup> in both models and observations (Fig. 2d and e).

a supprimé: . It

a supprimé: coasts

a supprimé: 4d

### 3.2 Projections of NPP and its environmental drivers



a supprimé:

**Figure 3.** CMIP6 projected pan-Arctic Ocean anomalies of NPP (a), surface NO<sub>3</sub> (b), SSIA (c) and SST (d) over the period 1900-2100 relative to 1850-1899, for the different emission scenarios. Vertical bars represent multi-model means and standard deviation in 2100. The last vertical bar and triangle represent the range and mean value for the CMIP5 RCP8.5 scenario in 2100. The numbers within parentheses in the legend give the number of available models. Additional figures representing the timeseries for subregions are shown in the appendix.

a supprimé: 5

a supprimé: in

a supprimé: of CMIP5

Across all SSPs, Arctic Ocean NPP and SST are projected to increase over this century, while nitrate concentration and IFSD decline (Fig. 3). However, the magnitude of change in each variable depends on the scenario, with generally larger anomalies and associated uncertainty under higher radiative forcing. An exception to this is SSP5-3.4, for which there is lower model uncertainty, possibly due to the smaller model ensemble (Fig. 6).

a supprimé: 5

a supprimé: of

a supprimé: 5

Projected Arctic Ocean NPP and nitrate inter-model uncertainty is greater than inter-scenario uncertainty by the end of the century (Fig. 3a and b). Contrary to the other variables, IFSD exhibits reduced uncertainty under higher radiative forcing scenarios. This reflects the strong model agreement that the Arctic Ocean will be ice-free for most months by the end of the century (Fig. 3c). Surface ocean warming shows significant sensitivity across scenarios, with the greatest warming (multi-model mean +4.78°C in 2081-2100), simulated in SSP5-8.5 (Fig. 6d).

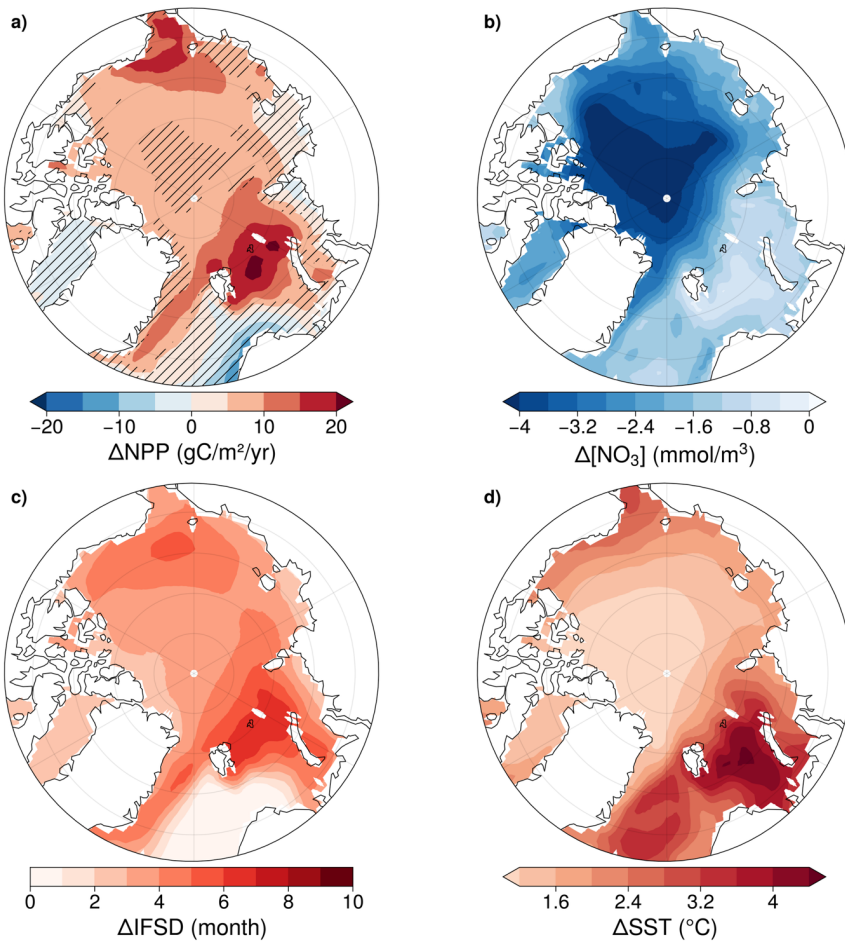
a supprimé: 5a

a supprimé: likely

a supprimé: almost

a supprimé: 5d

1 Projected twenty-first century NPP increases are highly divergent between CMIP6 and CMIP5 scenarios of comparable  
 2 high radiative forcing (Fig. 3a). For RCP8.5, the relative anomaly in NPP reaches  $11.5 \pm 15.7\%$  at the end of the century.  
 3 In contrast, SSP5-8.5 projects a much larger increase of  $46.4 \pm 53.7\%$ . This highlights greater CMIP6 model agreement  
 4 of increasing future NPP alongside a **more** than 3-fold increase in associated uncertainty (Fig. 3a). The projected twenty-  
 5 first century Arctic Ocean  $\text{NO}_3$  surface concentration decline is higher in SSP5-8.5 ( $4.38 \pm 1.98 \text{ mmol/m}^3$ ) than in RCP8.5  
 6 ( $3.09 \pm 1.45 \text{ mmol/m}^3$ , Fig. 3b). The increase in IFSD is **greater** in CMIP6 than in CMIP5 (7.8 months versus 4.2 months),  
 7 indicating a stronger reduction in sea-ice duration in CMIP6 compared to CMIP5. However, when expressed as anomalies  
 8 relative to the reference period, the magnitude of change is slightly lower in CMIP6 than in CMIP5 (Fig. 3c). The surface  
 9 ocean warming is two times higher in SSP5-8.5 ( $4.78 \pm 2.09 \text{ }^\circ\text{C}$ ) than in RCP8.5 ( $2.32 \pm 0.75 \text{ }^\circ\text{C}$ ) with higher associated  
 10 uncertainty (Fig. 3d).



- a supprimé: 5a
- a supprimé: ±
- a supprimé: %.
- a supprimé: ±
- a supprimé: greater
- a supprimé: 5a
- a supprimé: (-
- a supprimé: 5b
- a supprimé: larger
- a supprimé: 5d
- a supprimé: 5d
- a supprimé: ¶

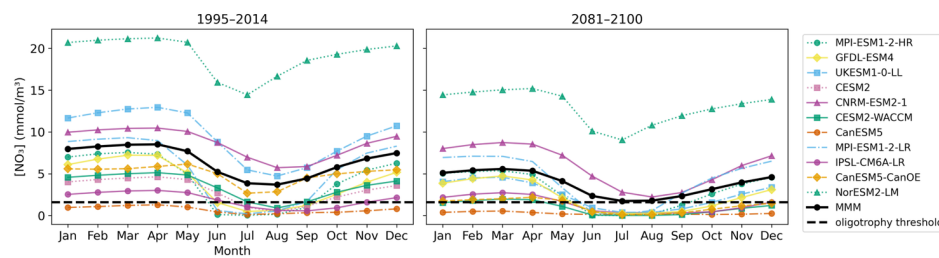
... [2]

11

1 **Figure 4:** CMIP6 multi-model mean anomalies of NPP (a), NO<sub>3</sub> (b), IFSD (c) and SST (d). Anomalies are for 2081-2100 of SSP5-8.5  
 2 relative to 1995-2014 of the historical simulation. **Hatched** areas indicate where <80% of the models agree on the sign of the change.

3 Multi-model mean declines in NO<sub>3</sub> and increases in IFSD and SST occur across the Arctic Ocean domain, however NPP  
 4 exhibits both regional-scale increases and decreases (Fig. 4a). NPP increases are greatest in the northern Barents Sea, along  
 5 the east coast of Greenland, and in the Chukchi Sea, reaching more than 20 gC/m<sup>2</sup>/yr. In contrast, **there are** NPP decreases  
 6 along the coast of the Kara Sea, in the North Atlantic, and in Baffin Bay (Fig. 4a). NO<sub>3</sub> concentration decreases across the  
 7 entire basin, with the most pronounced reductions **on** the Siberian shelf and off the East Siberian Shelf, **where declines can**  
 8 **exceed** 4 mmol/m<sup>3</sup> (Fig. 4b). The region experiencing the highest increase in the ice-free season duration is the northern  
 9 Barents Sea, east of Svalbard Archipelago. In the central **Arctic Basin**, sea ice **decline** is also strong, **with a loss of more**  
 10 **than 6 months ice coverage** (Fig. 4c). The Barents and Greenland Seas are the regions most affected by rising SST, with  
 11 **increases of up to 6°C** (Fig. 4d).

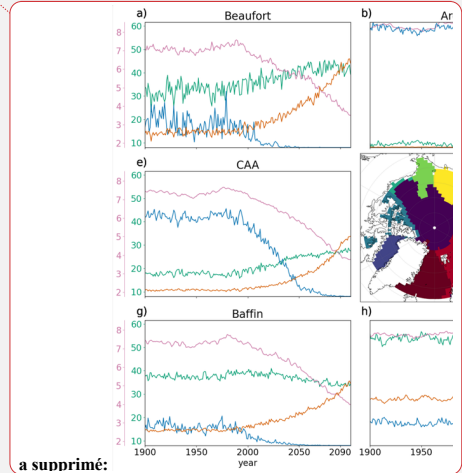
12 Most **models project consistent NPP increases** under SSP5-8.5 except over the shelves (where **anomalies are less**  
 13 **pronounced**) and in the **central Arctic Ocean**. For other variables, such as nitrate concentration, IFSD and SST, models  
 14 agree on the **sign of future change across the entire basin** (Fig. 4).



16 **Figure 5:** Seasonal cycle of nitrate concentration during the two last decades of the historical simulation (1995-2014) (left) and the  
 17 last two decades of SSP5-8.5 (2081-2100) (right). Each model is represented in a different color while the multi-model mean is shown  
 18 in black.

19 **By the end of the century, most CMIP6 models simulate a transition toward oligotrophic conditions, with an increasing**  
 20 **fraction of ensemble members exhibiting oligotrophy and longer seasonal persistence of these conditions** (Fig. 5). The  
 21 **seasonal cycle of nutrient concentration indicates that during the period 1995-2014, only seven CMIP6 models reach**  
 22 **oligotrophy during the productive period, generally from mid-May to September** (CanESM5, MPI-ESM1-2-LR, MPI-  
 23 **ESM1-2-HR, GFDL-ESM4, CESM2, CESM2-WACCM, and IPSL-CM6A-LR). An exception occurs for IPSL-CM6A-**  
 24 **LR, which remains oligotrophic until November, and for CanESM5, which is oligotrophic throughout the year. By the end**  
 25 **of the century, nine models reach oligotrophy (all except MPI-ESM1-2-HR and CNRM-ESM2-1), with duration extending**  
 26 **from early May to February. However, the multi-model mean is influenced by models with higher nutrient concentrations**  
 27 **and reaches oligotrophy only during July and August.**

- a supprimé: 6.
- a supprimé: Non-hatched
- a supprimé: 6
- a supprimé: 6a
- a supprimé: in of
- a supprimé: by more than
- a supprimé: 6b
- a supprimé: basin
- a supprimé: loss
- a supprimé: losing
- a supprimé: of annual
- a supprimé: cover
- a supprimé: 6c
- a supprimé: the SST increasing by
- a supprimé: 6d
- a supprimé: model are agreeing on the sign of
- a supprimé: variation
- a supprimé: the variation is low
- a supprimé: center of the
- a supprimé: sigh
- a supprimé: variation in
- a supprimé: whole
- a supprimé: 6



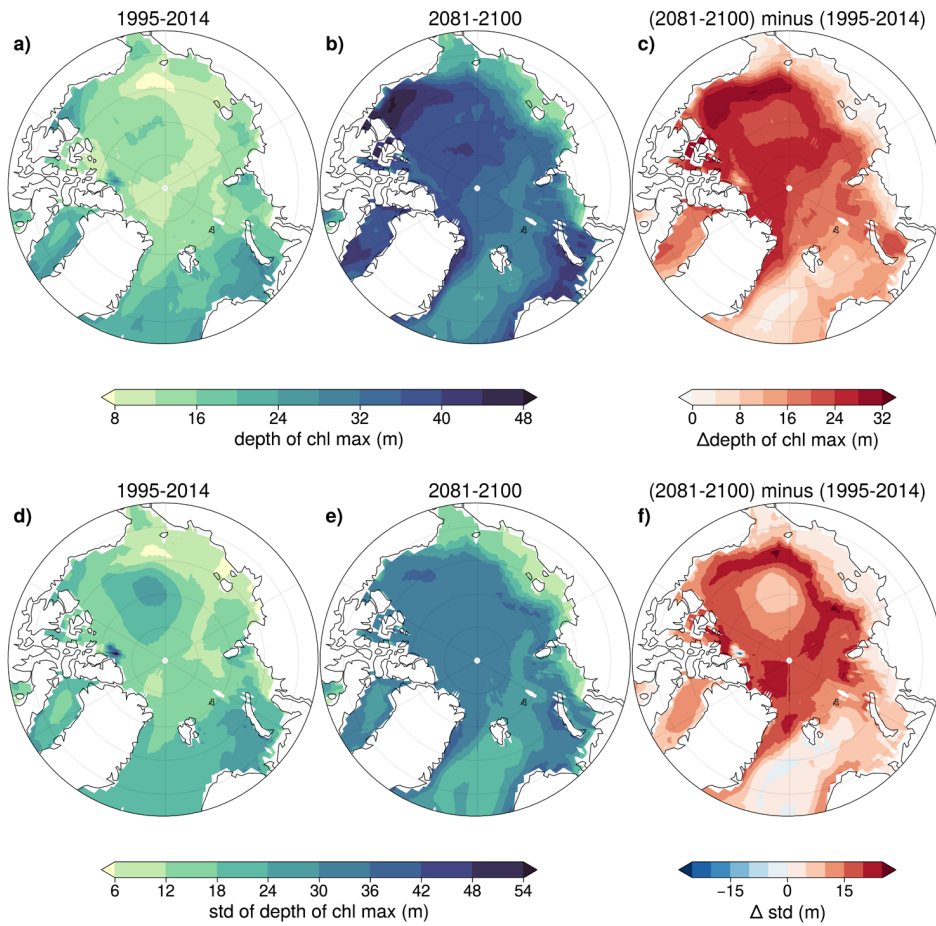
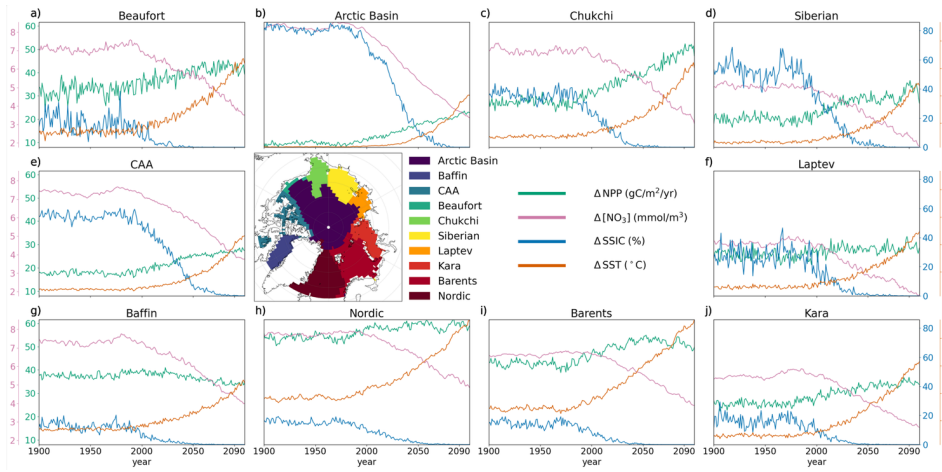


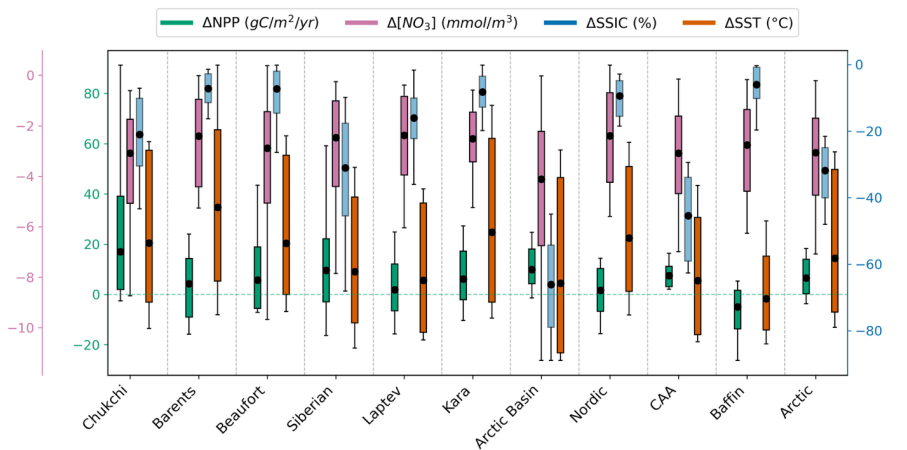
**Figure 6:** Depth of subsurface chlorophyll maximum (SCM) in July for the periods 1995–2014 (a) and 2081–2100 of SSP5-8.5 (b), and the difference between these two periods (c) (top row). Standard deviation of the July maximum chlorophyll depth across models for 1995–2014 (d), 2081–2100 of SSP5-8.5 (e), and the difference in standard deviation between these two periods (f) (bottom row).

The multi-model mean SCM deepens throughout the century across the Arctic Ocean, while the inter-model standard deviation increases (Fig. 6). During the period 1995–2014, the SCM is below 25 m over most of the Arctic Ocean, whereas it increases to up to 50 m by the end of the century, particularly in the Beaufort Sea and the central Arctic. A slight deepening is projected along the coastal regions of the Chukchi, Siberian, Laptev, and Kara seas.

Models largely disagree on the depth of the SCM, particularly in future projections where deepening is observed. In some regions, the uncertainty is nearly as high as the SCM depth, possibly indicating that while some models predict a deep SCM, others do not, consistent with findings from CMIP5 models (Steiner et al., 2016).



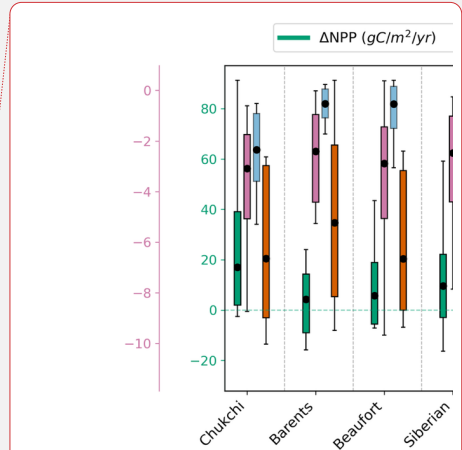
1  
2 **Figure 7.** CMIP6 multi-model mean basin-scale evolution of NPP (green),  $\text{NO}_3$  (pink), SSIC (blue) and SST (orange), over the period  
3 1900-2100 of the historical and SSP5-8.5 simulations, relative to 1850-1899.



4  
5 **Figure 8.** SSP5-8.5 ensemble anomalies of NPP (green),  $\text{NO}_3$  (pink), SSIC (blue) and SST (orange) for each Arctic basin and the entire  
6 Arctic Ocean domain. Each boxplot represents the multi-model mean, interquartile range and ensemble outliers in 2081-2100 relative  
7 to 1995-2014.

8 Across all Arctic sub-regions, multi-model mean NPP,  $\text{NO}_3$ , SSIC and SST are relatively stable until ~1980, after which  
9 all basins begin to exhibit varying levels of surface ocean warming alongside  $\text{NO}_3$  and SSIC declines (Fig. 7). The sign of  
10 regional-scale anomalies in  $\text{NO}_3$ , SSIC and SST is consistent across the CMIP6 ensemble, however model uncertainty  
11 varies across regions (Fig. 7 and 8).

12 The pan-Arctic Ocean  $\Delta\text{NPP}$  is relatively low compared to some other regions, with an ensemble range of  $-3.62 \text{ gC/m}^2/\text{yr}$   
13 to  $18.3 \text{ gC/m}^2/\text{yr}$  for the entire Arctic Ocean and  $-2.52$  to  $91.3 \text{ gC/m}^2/\text{yr}$  for the Chukchi Sea, where the increase and



a supprimé:

a supprimé: CMIP6

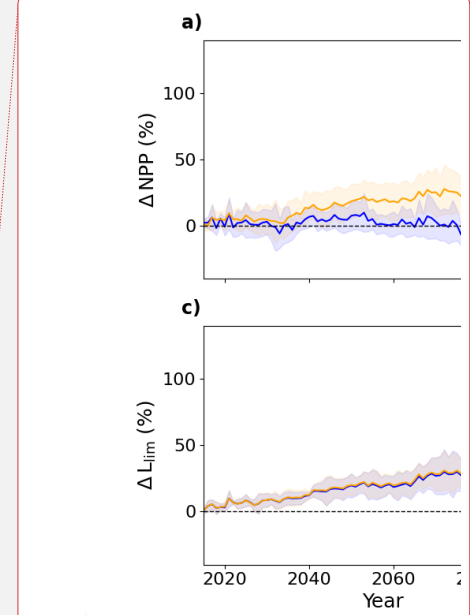
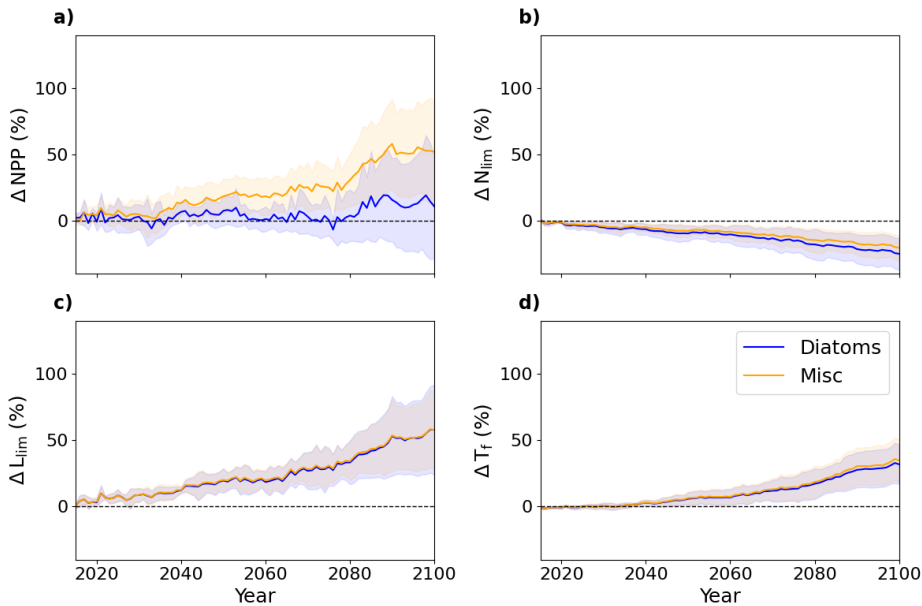
1 associated uncertainty is the highest. The decrease in NO<sub>3</sub> concentration is relatively consistent across Arctic sub-regions,  
2 ranging from approximately -2.38 mmol/m<sup>3</sup> in the Laptev Sea to -4.12 mmol/m<sup>3</sup> in the Arctic Basin. SST increases across  
3 all subregions, with an average increase of approximately 3.66°C across the entire Arctic Ocean. The highest multi-model  
4 ΔSST uncertainty is in the Barents Sea, with a model spread of 6.95°C, while the lowest uncertainty occurs in Baffin Bay,  
5 with a spread of 3.42°C (Fig. 8).

6 Baffin Bay differs from other regions as the only area where the multi-model mean NPP is projected to decline under SSP5-  
7 8.5. During the historical period (1995-2014), this subregion already has low annual mean sea ice coverage, therefore  
8 although it becomes ice-free by the end of the century under SSP5-8.5, the change in coverage remains small. Baffin Bay  
9 is also projected to experience the lowest multi-model mean surface ocean warming (2.53 °C) compared to other Arctic  
10 Ocean regions, with low uncertainty (Fig. 8).

11

- a supprimé: Temperature is rising
- a supprimé: basins
- a supprimé: whole
- a supprimé: annual temperature
- a supprimé: found
- a supprimé: basin
- a supprimé: September
- a supprimé: concentration, meaning that even though
- a supprimé: ocean
- a supprimé: a

1 **3.3 Phytoplankton growth limitation terms**

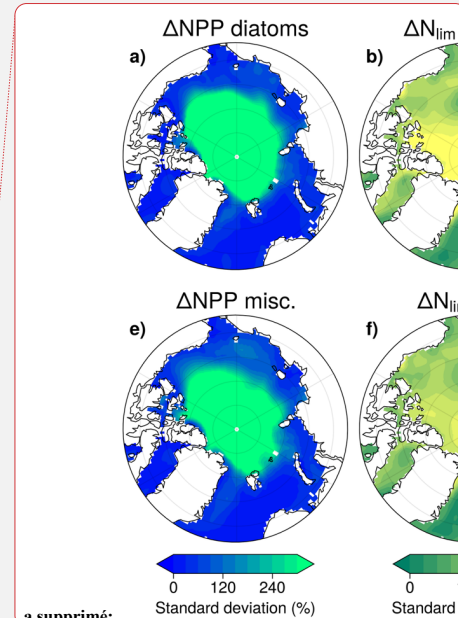
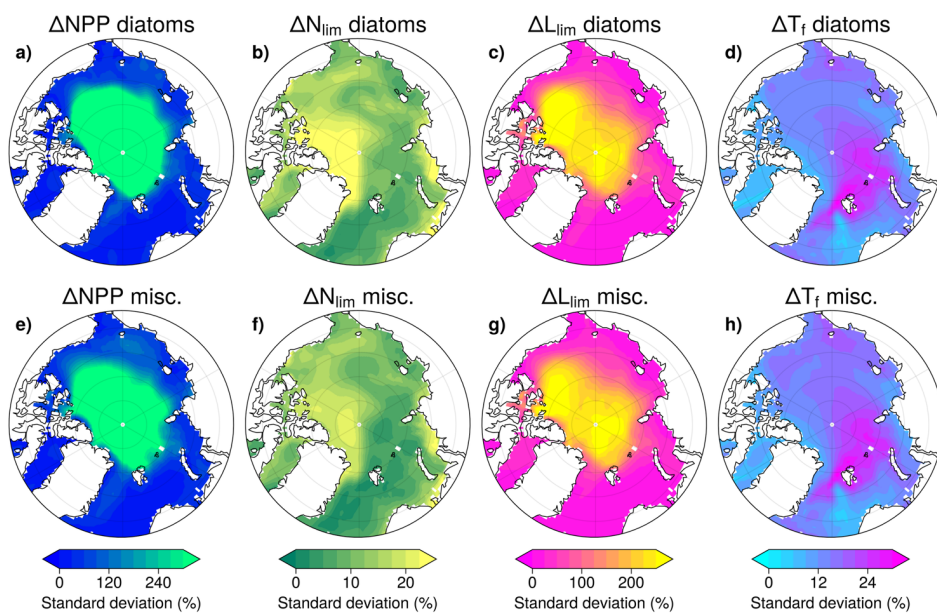


a supprimé:  
 a supprimé: and  
 a supprimé: uncertainty, represented as the  
 a supprimé: deviation are  
 a supprimé: over  
 a supprimé: contribution to  
 a supprimé: the  
 a supprimé: which is augmented by the influence of  
 a supprimé: on phytoplankton temperature functions and slightly ...  
 a supprimé: (Fig 9).  
 a supprimé: ±  
 a supprimé: ±  
 a supprimé: ±  
 a supprimé: confirmed by each  
 a supprimé: individually

2  
 3 **Figure 9.** Multi-model mean SSP5-8.5 pan-Arctic Ocean anomalies of diatom (blue) and miscellaneous phytoplankton (orange) NPP  
 4 (a), nutrient limitation (b), light limitation (c) and temperature function (d). Anomalies are relative to 1995-2014 values with the multi-  
 5 model standard deviations shaded.

6 As phytoplankton growth is the product of multiple limiting factors (Equation 1), the analysis of their relative anomalies  
 7 throughout the 21<sup>st</sup> century is necessary to assess their respective contributions to phytoplankton growth rate perturbations  
 8 and the projected increase in Arctic Ocean NPP. Diatoms exhibit a smaller increase in NPP compared to miscellaneous  
 9 phytoplankton, with respective increases of approximately 11% and 52% relative to 1995-2014. However, the uncertainty  
 10 associated with both groups is high and increases throughout SSP5-8.5 (Fig. 9a). The greatest driver of relative increases  
 11 in multi-model mean phytoplankton growth rates is a reduction in light limitation (Fig 9). Alongside this, warming directly  
 12 enhances growth rates via increases in  $T_f$  although this is offset by enhanced nutrient limitation. The  $L_{lim}$  and  $T_f$  increase  
 13 is consistent between PFTs (Fig. 9b, c). However, the  $\Delta L_{lim}$  uncertainty increases sharply, exceeding ±30% by 2100 for  
 14 both PFTs while  $\Delta T_f$  and  $\Delta N_{lim}$  uncertainty is between ±10% and ±20% by 2100 (Fig. 9b, c and d). Both PFTs are  
 15 increasingly nutrient limited in the Arctic Ocean over the 21<sup>st</sup> century, but diatoms are more impacted by nutrient  
 16 concentration declines (Fig. 9b). These trends are consistent across models (see Fig. A5).

17



a supprimé:

a supprimé: relative anomalies in NPP and phytoplankton growth limitation terms (Fig. 10).

a supprimé: PP

a supprimé: 6a

1

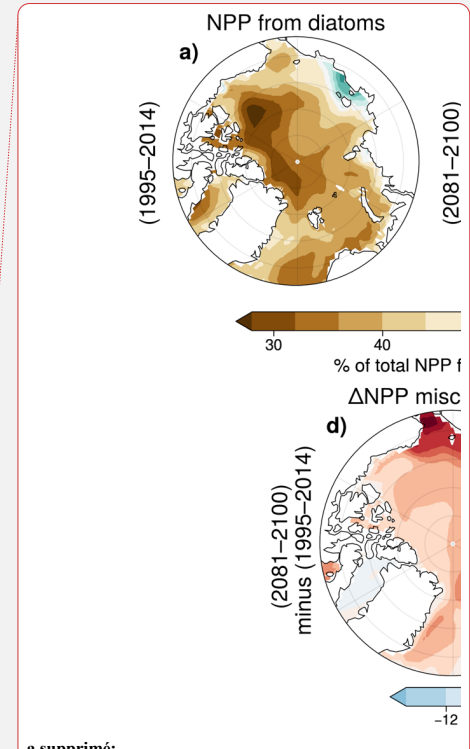
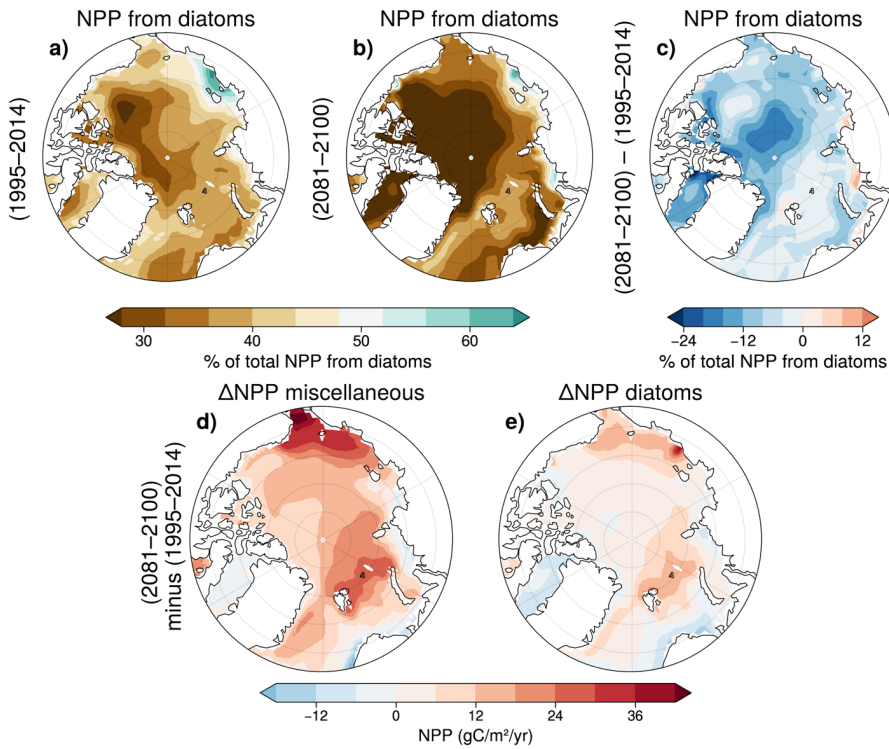
2 **Figure 10.** Regional differences in the multi-model standard deviation of anomalies in NPP (a, e), nutrient limitation (b, f), light  
3 limitation (c, g) and temperature function (d, h) in 2081-2100 of SSP5-8.5 relative to 1995-2014 of the historical. The upper row  
4 represents diatoms and the lower row miscellaneous phytoplankton.

5 To better understand NPP uncertainties, their causes and their distribution across the Arctic, we represented the multi-  
6 model standard deviation of SSP5-8.5 anomalies in NPP and growth limitation terms (Fig. 10). Diatoms and miscellaneous  
7 phytoplankton show comparable Arctic Ocean patterns of multi-model uncertainty associated with SSP5-8.5. Relative  
8  $\Delta NPP$  uncertainty is particularly pronounced in the central Arctic Ocean (Fig. 10a and e). This is coincident with the  
9 location of greatest  $\Delta L_{lim}$  uncertainty which reaches >210 % over the century in this region (Fig. 10c and g). In  
10 contrast,  $\Delta T_f$  and  $\Delta N_{lim}$  exhibit much lower uncertainty, remaining below 30 % across the entire Arctic Ocean (Fig. 10b,  
11 d, f and h). Given the very low  $\Delta NPP$  values in the Central Arctic Ocean, it is not surprising that the regions of greatest  
12 relative NPP uncertainty (central Arctic Ocean) differ from those exhibiting the largest absolute NPP increases (shelf  
13 regions, Fig. 4a).

14

15

16



1

2 **Figure 11.** Multi-model mean fraction of total NPP due to diatoms in 1995–2014 (a), and 2081–2100 under SSP5-8.5 (b). Change in %  
 3 of total NPP due to diatoms (c). Panels (d) and (e) show the anomalies in miscellaneous phytoplankton NPP (d), and diatom NPP (e) in  
 4 2081–2100 compared to 1995–2014.

5 In the two decades 1995–2014, diatoms are not the dominant contributor to total NPP across the majority of the Arctic  
 6 Ocean with the exception of the coastal East Siberian Sea where diatom NPP is particularly important (Fig. 11a). Under  
 7 SSP5-8.5, miscellaneous phytoplankton dominance is enhanced, notably in the central Arctic Ocean where they contribute  
 8 to up to 70 % of total NPP. In contrast, diatom NPP remains dominant in the coastal East Siberian Sea and exhibits  
 9 increasing dominance in the Kara and Laptev Seas (Fig. 11b).

10 The NPP increase is the greatest in Chukchi and Barents seas for both PFTs but highest for miscellaneous phytoplankton  
 11 (Fig. 11d, e). It confirms that the increase in total NPP in the pan-Arctic Ocean is driven mainly by enhanced productivity  
 12 of miscellaneous phytoplankton, rather than an increase in diatom productivity (Fig. 4). NPP of both PFTs, and in particular  
 13 diatom NPP, declines in the Baffin Bay, as well as in regions of the Nordic Seas and on the West Siberian shelf (Fig. 11d,  
 14 e).

a supprimé:

a supprimé: from

a supprimé: multi-model mean fraction of total NPP from diatoms in...

a supprimé: from

a supprimé: miscellaneous phytoplankton

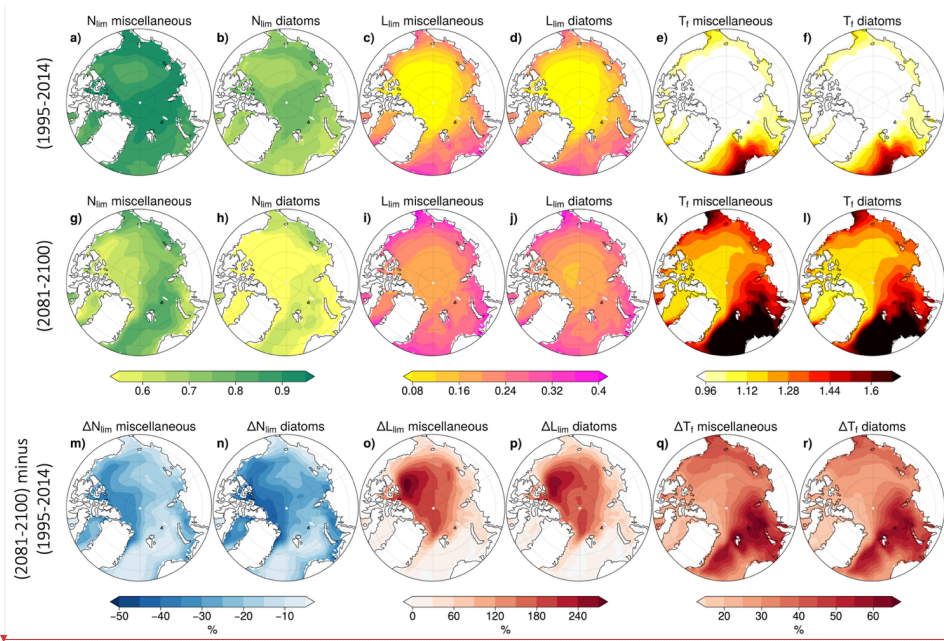
a supprimé: PFT

a supprimé: by diatoms

a supprimé: 6

a supprimé: parts

1



2

3 **Figure 12.** *CMP6* multi-model mean nutrient limitation, light limitation and temperature function for each PFT in 1995-2014 of the  
 4 historical simulation (top), 2081-2100 of *SSP5-8.5* (middle) and anomalies between these periods (bottom).

5 In the reference period (1995-2014),  $N_{lim}$  is lower for diatoms than for miscellaneous phytoplankton (Fig. 12a and b). This  
 6 is likely indicative of diatoms typically having higher nutrient half-saturation constants than nanophytoplankton in most  
 7 ocean biogeochemical models (e.g. Laufkötter et al., 2015). It could also be due to differences in the limiting nutrient but  
 8 this is unlikely given the agreement between the spatial distributions of  $N_{lim}$  and  $\Delta N_{lim}$  for each phytoplankton type (Fig.  
 9 12m and n). In the Canadian Basin and in Baffin Bay, diatom  $N_{lim}$  decreases by over 40 %, with changes in diatom growth  
 10 rate dominated by  $N_{lim}$  anomalies. For miscellaneous phytoplankton, nutrient limitation is also enhanced but to a lesser  
 11 extent, with a maximum  $N_{lim}$  decrease below 20 % (Fig. 12m and n).

12 For both PFTs,  $L_{lim}$  and  $T_f$  exhibit similar regional distributions during the reference period (1995-2014).  $L_{lim}$  is highest in  
 13 the Nordic and Barents Seas, reaching 0.4, while  $T_f$  is also highest in these regions with values exceeding 1.8. Conversely,  
 14 both  $L_{lim}$  and  $T_f$  show their lowest values in the Arctic Basin (Fig. 12c, d, e, and f). The temporal evolution of these terms  
 15 is consistent between PFTs.  $L_{lim}$  increases most substantially in the central Arctic, with an increase of approximately 180%  
 16 relative to the reference period (Fig 12o and p) demonstrating strong alleviation of light limitation, while  $T_f$  increases are  
 17 most pronounced in the Kara Sea, Barents Sea, and Nordic Seas, exceeding 50% relative to the reference period (Fig 12q  
 18 and r).

a supprimé:

a supprimé: state

a supprimé: ) and anomalies in

a supprimé: 12Figure a

a supprimé: (e.g. Laufkötter et al., 2015).

a supprimé: indicating that

a supprimé: are

a supprimé: Light limitation factor

a supprimé: temperature factors

a supprimé: peak

a supprimé: at

a supprimé: evolutionary patterns

a supprimé: remain

a supprimé: , though their spatial distributions of change differ...

a supprimé: showing a

a supprimé: the temperature factor

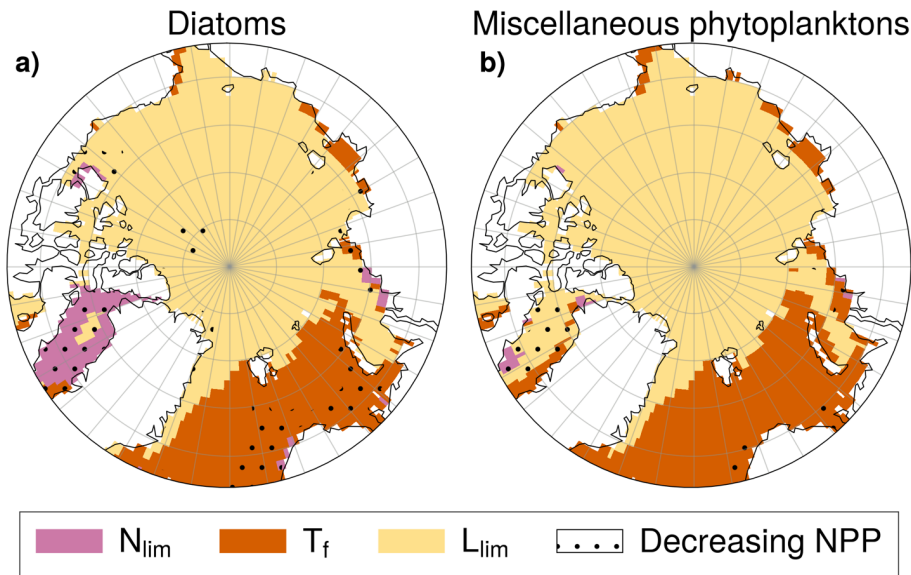
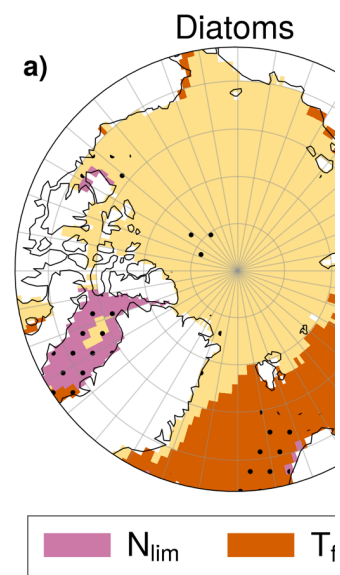


**Figure 13.** Dominant driver of phytoplankton growth rate changes ( $\Delta\mu$ ) in SSP5-8.5 for diatoms (a) and miscellaneous phytoplankton (b). Colors denote whether  $L_{lim}$  (yellow),  $T_f$  (orange) or  $N_{lim}$  (pink) is the largest contributor to  $\Delta\mu$ . NPP anomalies are negative in stippled areas and positive elsewhere.

In SSP5-8.5 simulations, increasing  $L_{lim}$  (reduced light limitation) is the principal driver of multi-model mean increases in phytoplankton growth rates for both diatoms and miscellaneous phytoplankton across the Arctic Ocean, particularly in the central Arctic where this is coincident with NPP increases (Fig. 13). In the Nordic, Barents, and Kara Seas, phytoplankton growth rate changes of both PFTs are mainly driven by increasing  $T_f$  (thermal enhancement) and generally consistent with NPP increases, except off the Norwegian coast. In contrast, in Baffin Bay, declining  $N_{lim}$  (greater nutrient limitation) is the dominant contributor to growth rate changes for diatoms and is consistent with declining diatom NPP (see Fig. A6, A7, A8, A9). For miscellaneous phytoplankton however, increasing  $L_{lim}$  is the dominant contributor to growth rate changes. This is indicative of enhanced growth rates but miscellaneous phytoplankton NPP is projected to decline in Baffin Bay (Fig. 13b). This suggests that other mechanisms, such as enhanced zooplankton grazing rates (Rohr et al., 2023) may contribute to projected NPP declines in this region.

#### 4. Discussion

Projected twenty-first century increases in Arctic Ocean NPP are higher and more variable in CMIP6 than in CMIP5. The multi-model mean NPP increase is four times larger under comparable high radiative forcing in CMIP6 than in CMIP5 (respectively 46.4 % and 11.5 % compared to the historical period, see Fig. 6a), with uncertainty at the end of the century three times higher in CMIP6 than CMIP5, consistent with previous studies (Tagliabue et al. 2021). The CMIP6 and CMIP5 ensembles also exhibit differing temporal evolution of NPP over the course of the 21<sup>st</sup> century. All CMIP6 models exhibit monotonic increases in Arctic Ocean NPP, whereas CMIP5 models exhibit more diverse responses, with some models showing an initial increase in NPP followed by a subsequent decrease due to the emergence of oligotrophic conditions (Vancoppenolle



a supprimé:

a supprimé: Area where

a supprimé: are

a supprimé: contributor

Code de champ modifié

a supprimé: 4. Discussion  
 Projected twenty-first century increases in Arctic Ocean NPP are higher and more variable in CMIP6 than in CMIP5. The multi-model mean NPP increase is four times larger under comparable high radiative forcing in CMIP6 than in CMIP5 (respectively 46.4 % and 11.5 % compared to the historical period, see Fig. 5a), with uncertainty at the end of the century three times higher in CMIP6 than CMIP5, consistent with previous studies (Tagliabue et al. 2021). The CMIP6 and CMIP5 ensembles also exhibit a different temporal evolution of NPP over the course of the 21<sup>st</sup> century. All CMIP6 models exhibit monotonic increases in Arctic Ocean NPP, whereas CMIP5 models exhibit more diverse responses, with some models showing an initial increase in NPP followed by a subsequent decrease due to the emergence of oligotrophic conditions (Vancoppenolle et al. 2013). In absolute terms, the most substantial NPP increases in CMIP6 are observed in the inflow shelf regions, that experience the greatest warming, sustained nutrient levels and limited change in light availability. This is consistent with the trend in the current observations (Lewis et al., 2020). The model uncertainty associated with CMIP6 Arctic Ocean NPP projections is higher than the scenario uncertainty (Fig. 3). This result is consistent with global NPP projections, which indicates finely balanced limitations on NPP, which often compensate one another (Bopp et al., 2013; Kwiatkowski et al., 2020). The direct influence and balance among climate-driven drivers of phytoplankton growth rates, namely temperature, light and nutrient availability, shifts substantially in CMIP6 compared to CMIP5. The stronger Arctic Ocean surface

1 [et al. 2013](#)). In absolute values, the most substantial NPP increases in CMIP6 are observed in the inflow shelf regions,  
2 [which experience the greatest warming, sustained nutrient levels and limited change in light availability. This is consistent](#)  
3 [with the trend in the current observations \(Lewis et al., 2020\). The model uncertainty associated with CMIP6 Arctic Ocean](#)  
4 [NPP projections is higher than the scenario uncertainty \(Fig. 3\). This result is consistent with global NPP projections, which](#)  
5 [indicates finely balanced limitations on NPP, which often compensate one another \(Bopp et al., 2013; Kwiatkowski et al.,](#)  
6 [2020\).](#)

7 [The direct influence and balance among climate-driven drivers of phytoplankton growth rates, namely temperature, light](#)  
8 [and nutrient availability, shifts substantially in CMIP6 compared to CMIP5. The stronger Arctic Ocean surface warming](#)  
9 [projected in CMIP6 and greater associated uncertainty \(Fig. 6\) relates to higher and more variable climate sensitivity](#)  
10 [\(Zelinka et al., 2020\) with similar Arctic amplification simulated across both ensembles \(Hahn et al., 2021\). This results in](#)  
11 [greater thermally-driven increases in phytoplankton growth rates than previously simulated in CMIP5 \(Laufkötter et al.,](#)  
12 [2015; Nakamura & Oka, 2019\). The more pronounced Arctic Ocean sea ice loss in CMIP6 \(Notz & Community, 2020\)](#)  
13 [increases light availability in the upper ocean, thereby further acting to enhance phytoplankton growth rates and associated](#)  
14 [NPP. In addition to this intensified sea ice loss, a number of CMIP6 models include an improved representation of sea ice](#)  
15 [light attenuation, resulting in generally higher under-ice light transmission \(Lebrun et al., 2023\). Although CMIP6](#)  
16 [simulations exhibit a larger decrease in upper Arctic Ocean nitrate concentrations over the 21<sup>st</sup> century \(Fig. 6b\),](#)  
17 [oligotrophic conditions are reached later and less frequently compared to CMIP5 models \(Vancoppenolle et al., 2013\), due](#)  
18 [to higher simulated mean state nutrient concentrations.](#)

19 [Beyond changes in mean nutrient concentration, CMIP6 projections point to a reorganization of the seasonal dynamics of](#)  
20 [nutrient limitation throughout the century in the Arctic Ocean. The lengthening of the oligotrophic period in CMIP6](#)  
21 [projections suggests a progressive extension of nutrient limitation beyond the peak bloom phase, potentially affecting both](#)  
22 [the magnitude and the phenology of phytoplankton production \(Manizza et al., 2023\). The intensity of the bloom is](#)  
23 [constrained by the seasonal depletion of nutrients, despite enhanced light availability and warmer temperatures, while a](#)  
24 [delayed replenishment in autumn and winter could limit the recovery of nutrient inventories prior to the following growing](#)  
25 [season. Contrary to expectations, nutrient replenishment is not occurring in autumn despite the expansion of open water](#)  
26 [areas. Under usual conditions, the reduced sea ice cover in this season would increase fetch, which could allow stronger](#)  
27 [storm-driven mixing and entrain nutrient-rich deep waters into the surface layer \(Ardyna et al., 2014\). Our analysis suggests](#)  
28 [that if his phenomenon is occurring, it is inefficient.](#)

29 Although NPP is projected to increase in most regions of the Arctic Ocean, many models simulate local declines,  
30 particularly in Baffin Bay and [in](#) the Nordic Seas. These regions are characterized by rising temperatures, reduced nutrient  
31 availability and little or no sea ice in present-day conditions. As such, the potential for changes in light supply is low in  
32 these areas and phytoplankton growth shows little to no increase due to increased light availability. While higher  
33 temperatures do stimulate growth rates, the limiting effect of declining nutrient availability dominates, resulting in overall  
34 NPP declines in Baffin Bay and Nordic Seas. The projected decline in NPP in Baffin Bay is consistent with recent  
35 observations of decreasing productivity in this region ([Ardyna & Arrigo, 2020](#)).

36 [In addition to this projected NPP increase, in CMIP6 models, the SCM deepens in CMIP6, consistent with CMIP5 \(Steiner](#)  
37 [et al., 2016\). However, the uncertainty associated with this deepening is high and the modeled historical SCM depth is still](#)  
38 [inconsistent with observational estimates.](#)

**a supprimé:** (Ardyna & Arrigo, 2020)

**a supprimé:** Arctic Ocean phytoplankton communities are projected to shift toward smaller size classes, with miscellaneous phytoplankton increasingly dominating primary production throughout the 21st century (Fig. 11). This change in phytoplankton community structure aligns with previous projections from ESMs (Bopp et al., 2005; Fu et al., 2016), and is driven by differential nutrient affinities among PFTs. Miscellaneous phytoplankton demonstrate greater competitive advantage than diatoms under the increasingly low-nutrient conditions (Ward et al., 2012). In most of the Arctic Basin where NPP is increasing, productivity exhibits substantial gains, with miscellaneous phytoplankton driving most of this enhancement. This production is facilitated by newly ice-free waters that provide increased light availability and extended growing seasons. In contrast, in Baffin Bay and Nordic Seas, the decline of NPP is driven by a pronounced decrease in diatom productivity. While smaller miscellaneous phytoplankton can efficiently exploit low-nutrient environments and capitalize on higher temperatures, larger diatoms require higher nutrient concentrations to maintain their growth (Marinov et al., 2010). These contrasting patterns suggest a fundamental shift in Arctic marine ecosystems, with implications for higher trophic levels and thus carbon pump efficiency (Grebmeier et al., 2010; Ward et al., 2012).  
In particular, a transition toward smaller phytoplankton cells is expected to reduce the efficiency of energy transfer to zooplankton, especially large lipid-rich copepods such as *Calanus glacialis* and *C. hyperboreus*, which development depends on the timing and magnitude of diatom-dominated blooms for feeding and reproduction (Leu et al., 2011; Wassmann, 2011). Such temporal mismatches can cascade through the food web, affecting the growth, recruitment and distribution of key predators including fish, seabirds and marine mammals (Haug et al., 2017). Moreover, although export production is not assessed in this study, reduced export of large, fast-sinking diatom aggregates may weaken pelagic-benthic coupling, ultimately altering benthic communities and their role in carbon remineralization (Wassmann et al., 2006).  
This study highlights the complexity of projecting future NPP in the Arctic Ocean under anthropogenic pressure. While Arctic Ocean NPP is projected to increase throughout the 21st century, substantial uncertainties persist alongside pronounced spatial heterogeneity, with diverse impacts.

1 Arctic Ocean phytoplankton communities are projected to shift toward smaller size classes, with miscellaneous  
2 phytoplankton increasingly dominating primary production throughout the 21st century (Fig. 11). This change in  
3 phytoplankton community structure aligns with previous projections from ESMs (Bopp et al., 2005; Fu et al., 2016), and  
4 is driven by differential nutrient affinities among PFTs. Miscellaneous phytoplankton demonstrate greater competitive  
5 advantage than diatoms under the increasingly low-nutrient conditions (Ward et al., 2012). In most of the Arctic Basin  
6 where NPP is increasing, productivity exhibits substantial gains, with miscellaneous phytoplankton driving most of this  
7 enhancement. This production is facilitated by newly ice-free waters that provide increased light availability and extended  
8 growing seasons. In contrast, in Baffin Bay and Nordic Seas, the decline of NPP is driven by a pronounced decrease in  
9 diatom productivity. While smaller miscellaneous phytoplankton can efficiently exploit low-nutrient environments and  
10 capitalize on higher temperatures, larger diatoms require higher nutrient concentrations to maintain growth (Marinov et al.,  
11 2010). These contrasting patterns suggest a fundamental shift in Arctic marine ecosystems, with implications for higher  
12 trophic levels and thus carbon pump efficiency (Grebmeier et al., 2010; Ward et al., 2012).

13 In particular, a transition toward smaller phytoplankton cells is expected to reduce the efficiency of energy transfer to  
14 zooplankton, especially large lipid-rich copepods such as *Calanus glacialis* and *Calanus hyperboreus*, whose development  
15 depends on the timing and magnitude of diatom-dominated blooms for feeding and reproduction (Leu et al., 2011;  
16 Wassmann, 2011). Such temporal mismatches can cascade through the food web, affecting the growth, recruitment and  
17 distribution of key predators including fish, seabirds and marine mammals (Haug et al., 2017). Moreover, although export  
18 production is not assessed in this study, reduced export of large, fast-sinking diatom aggregates may weaken pelagic–  
19 benthic coupling, ultimately altering benthic communities and their role in carbon remineralization (Wassmann et al.,  
20 2006).

21 This study highlights the complexity of projecting future NPP in the Arctic Ocean under anthropogenic pressure. While  
22 Arctic Ocean NPP is projected to increase throughout the 21st century, substantial uncertainties persist alongside  
23 pronounced spatial heterogeneity, with diverse impacts. The projected shift in phytoplankton community structure toward  
24 smaller taxa may exacerbate the weakening of the Arctic Ocean carbon sink, which is already projected to decline due to  
25 surface ocean warming that reduces CO<sub>2</sub> solubility and enhances stratification (Oziel et al., 2025). Concurrently, these  
26 ecosystem changes could cause unclear impacts to local communities, whose economic livelihoods, food security, public  
27 health, and cultural identity depend heavily on marine resources (Malik & Ford, 2025; Mudryk et al., 2021). The magnitude  
28 and spatial distribution of future NPP changes remain highly uncertain due to differences in key limiting factors,  
29 biogeochemical parameterizations and their impact on phytoplankton community structure. In particular, the limited  
30 representation of sea-ice algae in most CMIP6 models might affect the phenology of pan-Arctic NPP as well as its vertical  
31 distribution and associated carbon export. Specifically, uncertainties in light penetration through varying sea ice thickness  
32 and optical properties, coupled with incomplete understanding of nutrient availability and cycling beneath ice-covered  
33 waters, represent critical knowledge gaps. Improving future Arctic Ocean NPP simulations requires enhanced  
34 representation of present-day nutrient levels, more accurate light transmission parameterizations through sea ice, and  
35 reduced climate sensitivity uncertainties across model ensembles.

a supprimé: will

a supprimé: (Oziel et al., 2025)

a supprimé: (Malik & Ford, 2025; Mudryk et al., 2021)

1 **5. Conclusion**

2 The increase in Arctic Ocean NPP projected by CMIP6 models for the end of the 21st century under high anthropogenic  
 3 emissions is about four times higher than in CMIP5. This is mostly due to the higher climate sensitivity of CMIP6 models,  
 4 leading to greater warming and earlier September sea-ice loss and a longer open-water season, together with a lower  
 5 limitation by nutrients. CMIP6 models also incidentally simulate higher nutrient levels than their CMIP5 counterparts. The  
 6 NPP increase is accompanied by a shift toward smaller phytoplankton species, driven by projected nutrient decline over  
 7 the 21st century — despite CMIP6 models simulating higher absolute nutrient levels than CMIP5. This community shift  
 8 has implications for higher trophic levels, biogeochemical cycling, and carbon export. The implications for ecosystem  
 9 services and indigenous communities that depend on marine resources remain largely unassessed.

a supprimé: stronger

a supprimé: in the phytoplankton community

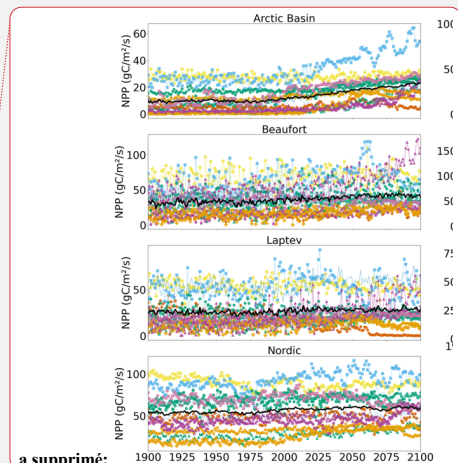
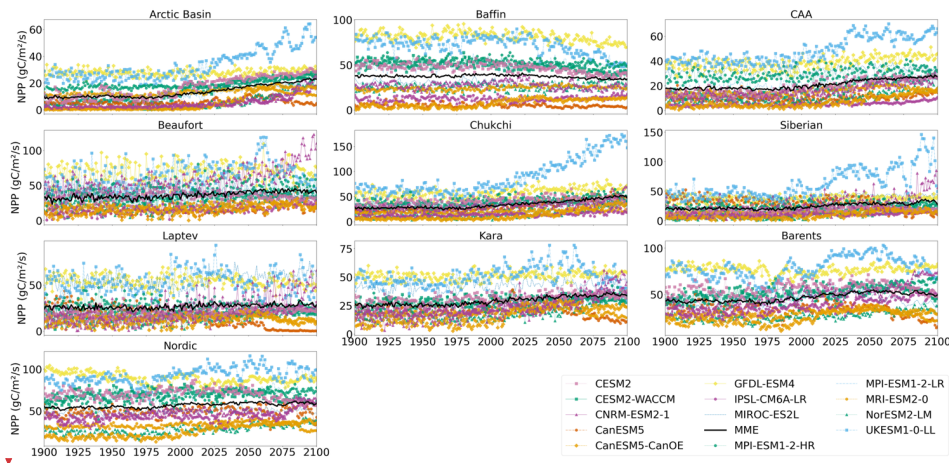
a supprimé: — more competitive under low-

a supprimé: conditions — with impacts on

a supprimé: Implications

a supprimé: Indigenous

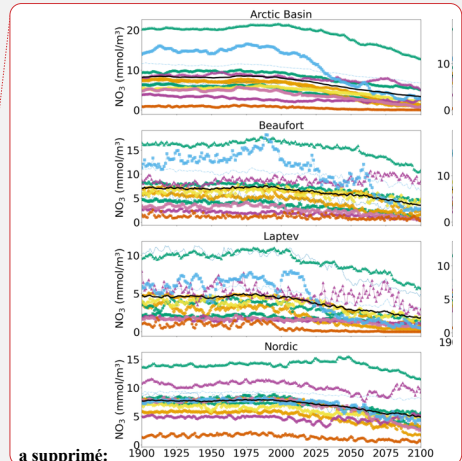
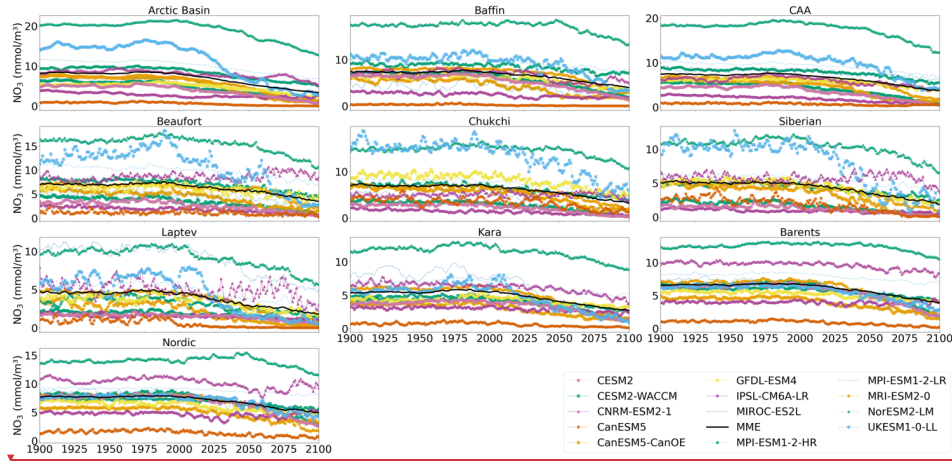
10 **Appendix A: Analyses of individual models**



a supprimé:

a supprimé: .

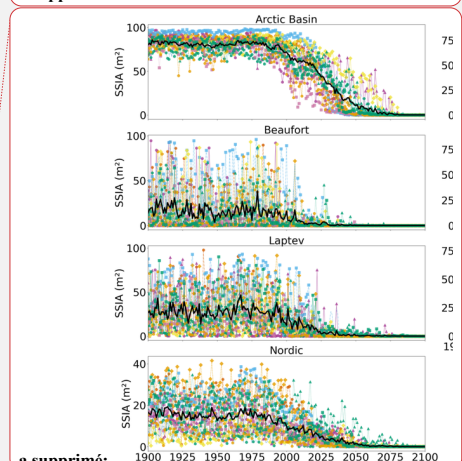
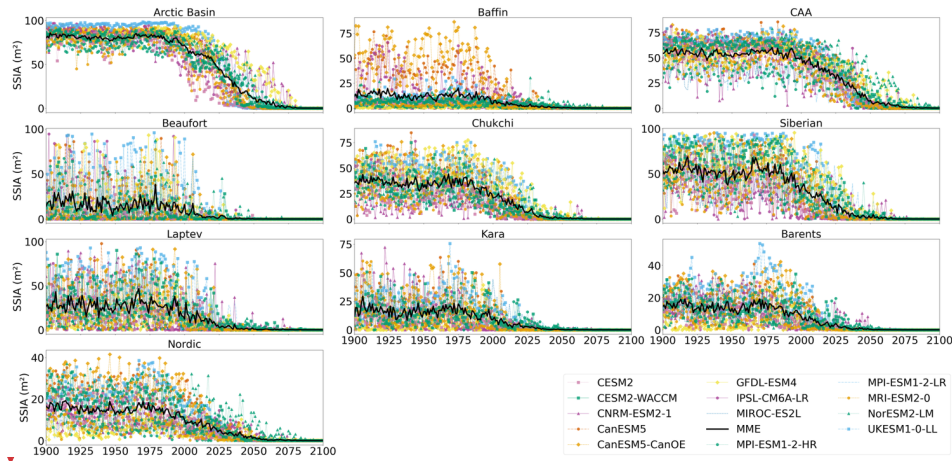
11 **Figure A1:** Projected regional annual mean NPP during the period 1900-2100, (historical and SSP5-8.5). Multi-model mean is shown  
 12 in black.  
 13



a supprimé:

a supprimé: in MLD

a supprimé: .

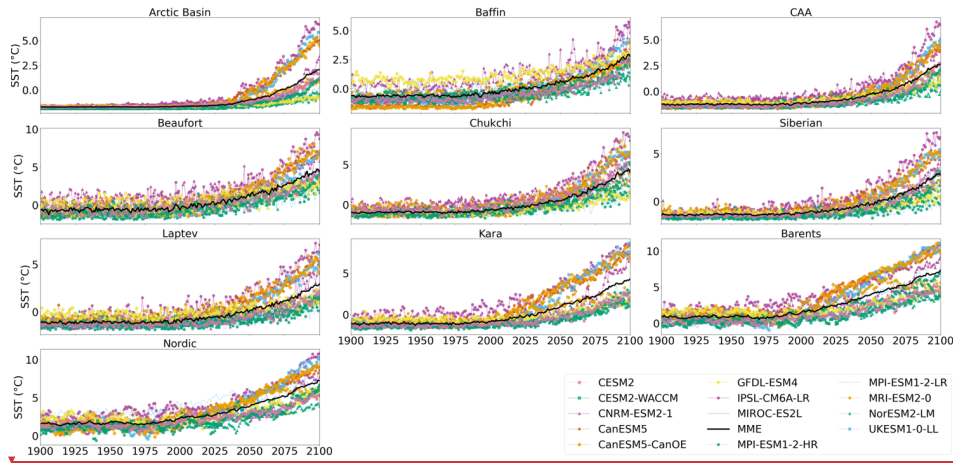


a supprimé:

a supprimé: .

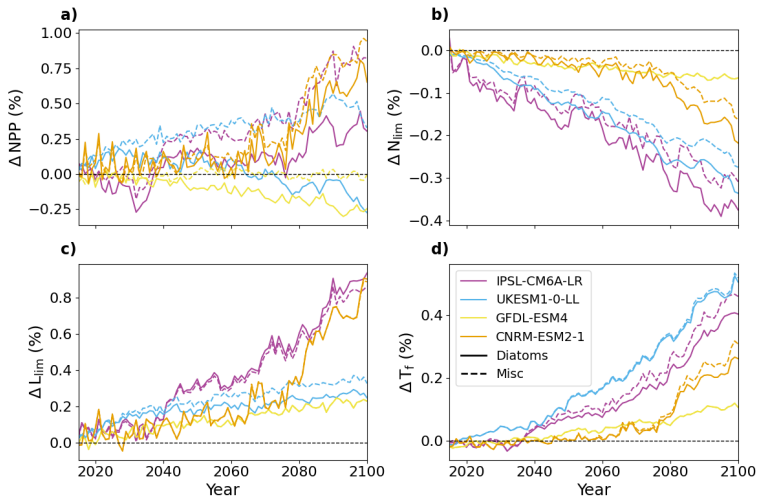
1  
2 **Figure A2:** Projected regional annual mean *MLD NO3* concentration during the period 1900-2100, (historical and SSP5-8.5). Multi-  
3 model mean is shown in black.

4  
5 **Figure A3:** Projected regional September sea ice concentration during the period 1900-2100, (historical and SSP5-8.5). Multi-  
6 model mean is shown in black.

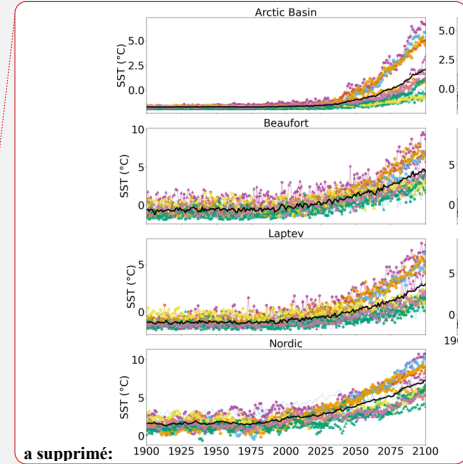


1

2 **Figure A4:** Projected regional SST during the period 1900-2100 (historical and SSP5-8.5). Multi-model mean is shown in black

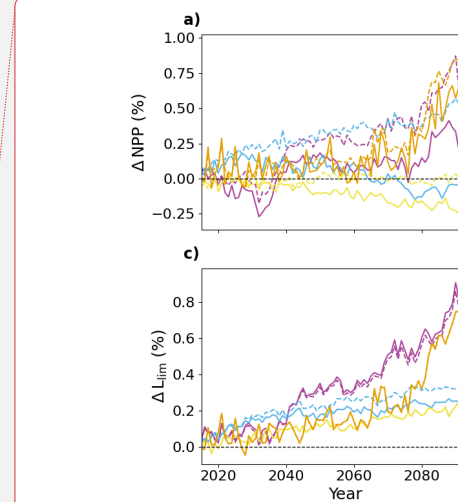


3



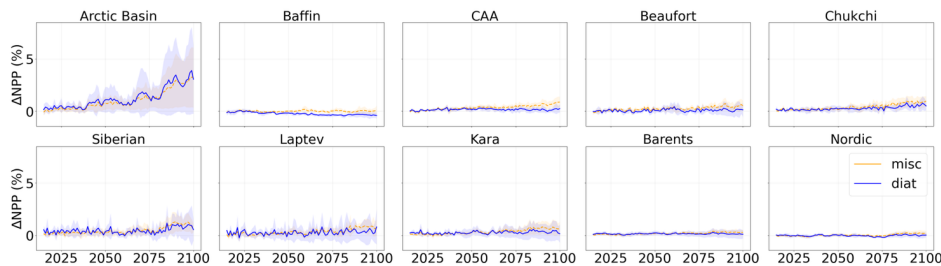
a supprimé:

a supprimé :

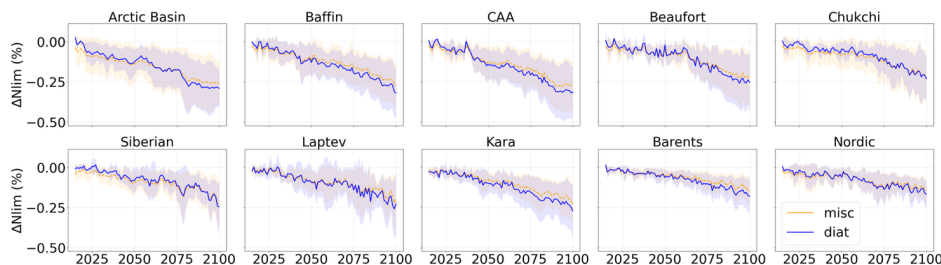


a supprimé:

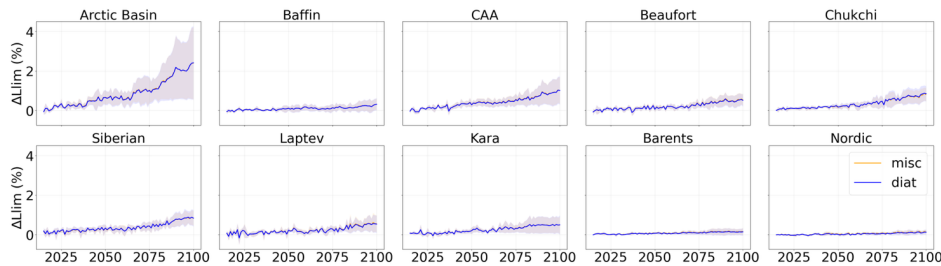
1 **Figure A5:** Evolution of *SSP5-8.5* NPP (a),  $N_{lim}$  (b),  $L_{lim}$  (c) and  $T_f$  (d) for each model and each PFT, relative to the period 1995-2014  
 2 averaged over the pan-Arctic Ocean.



3  
 4 **Figure A6:** Projected NPP relative to 1995-2014 during the period 2015-2100 of *SSP5-8.5* in each subregion of the Arctic Ocean.  
 5 Diatoms are represented in blue and miscellaneous phytoplankton in orange. Shading represents the multi-model standard deviation.



6  
 7 **Figure A7:** Projected nutrient limitation factor relative to 1995-2014 during the period 2015-2100 of *SSP5-8.5* in each  
 8 subregion of the Arctic Ocean. Diatoms are represented in blue and miscellaneous phytoplankton in orange. Shading represents the  
 9 multi-model standard deviation.

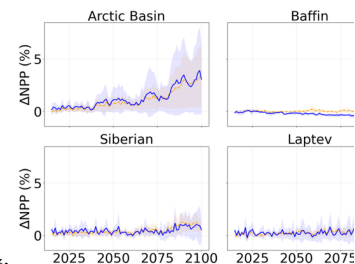


10  
 11 **Figure A8:** Projected light limitation factor relative to 1995-2014 during the period 2015-2100 of *SSP5-8.5* in each subregion of the  
 12 Arctic Ocean. Diatoms are represented in blue and miscellaneous phytoplankton in orange. Shading represents the multi-model  
 13 standard deviation.



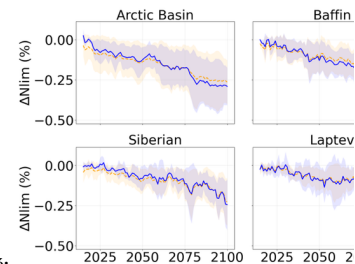
a supprimé: in

a supprimé: Model are shown in different color, diatoms in solid line and miscellaneous phytoplankton in dash line.



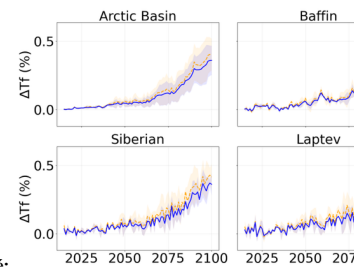
a supprimé:

a supprimé: basin



a supprimé:

a supprimé: basin of the Arctic Ocean. Diatoms are represented in blue and miscellaneous phytoplankton in orange. Shading represents the multi-model standard deviation. [4]

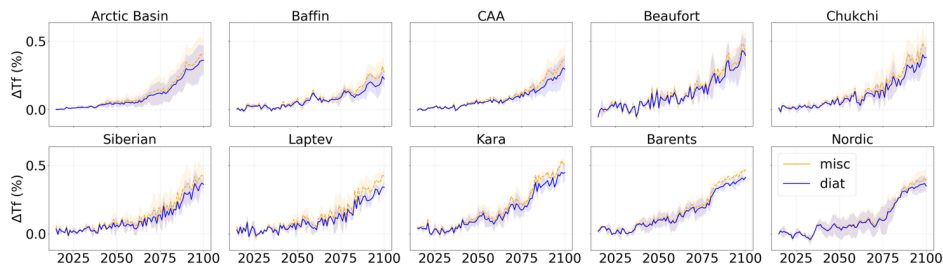


a supprimé:

a supprimé: A9

a supprimé: temperature function

a supprimé: basin



1  
2 **Figure A9:** Projected temperature function relative to 1995-2014 during the period 2015-2100 of SSP5-8.5 in each subregion of the  
3 Arctic Ocean. Diatoms are represented in blue and miscellaneous phytoplankton in orange. Shading represents the multi-model standard  
4 deviation.

5  
6 **Code data and availability**

7 Publicly available datasets were analysed in this study. This data can be found at <https://esgf.llnl.gov/> (last access:  
8 December 2025)(Earth System Grid Federation, 2025).

9 Codes are available upon request to the corresponding author LCB.

10 **Acknowledgements**

11 We gratefully acknowledge the ClimArctic project for supporting and enabling this study, as well as Olivier Torres for his  
12 help in processing the CMIP6 output data. This work was supported by a French government grant managed by the Agence  
13 Nationale de la Recherche under the France 2030 program (project CLIMArctic, reference ANR-22-POCE-0005).

14 **Author contribution**

15 LK, MV and LCB conceived the study. LCB did the analysis and wrote the paper.

16 **References**

17 Ardyna, M., & Arrigo, K. R. (2020). Phytoplankton dynamics in a changing Arctic Ocean. *Nature Climate Change*, *10*(10),  
18 892-903. <https://doi.org/10.1038/s41558-020-0905-y>

19 Ardyna, M., Babin, M., Gosselin, M., Devred, E., Rainville, L., & Tremblay, J.-É. (2014). Recent Arctic Ocean sea ice loss  
20 triggers novel fall phytoplankton blooms. *Geophysical Research Letters*, *41*(17), 6207-6212.  
21 <https://doi.org/10.1002/2014GL061047>

22 Arrigo, K. R., & van Dijken, G. L. (2015). Continued increases in Arctic Ocean primary production. *Progress in*  
23 *Oceanography, Synthesis of Arctic Research (SOAR)*, *136*, 60-70. <https://doi.org/10.1016/j.pocean.2015.05.002>

24 Bopp, L., Aumont, O., Cadule, P., Alvain, S., & Gehlen, M. (2005). Response of diatoms distribution to global warming  
25 and potential implications: A global model study. *Geophysical Research Letters*, *32*(19).  
26 <https://doi.org/10.1029/2005GL023653>

a supprimé: 2011). Secular trends

a supprimé: net

a supprimé: Journal

a supprimé: *Geophysical Research: Oceans*, *116*(C9).  
<https://doi.org/10.1029/2011JC007151>

Bentsen, M., Bethke, I., Debernard, J. B., Iversen, T.,  
Kjirkevåg, A., Seland, Ø., Drange, H., Roelandt, C., Seierstad,  
I. A., Hoose, C., & Kristjánsson, J. E. (2013). The Norwegian  
Earth System Model, NorESM1-M – Part 1 : Description and  
basic evaluation of the physical climate. *Geoscientific Model  
Development*, *6*(3), 687-720.

a supprimé: 5194/gmd-6-687-2013

1 Bopp, L., Resplandy, L., Orr, J. C., Doney, S. C., Dunne, J. P., Gehlen, M., Halloran, P., Heinze, C., Ilyina, T., Séférian,  
2 R., Tjiputra, J., & Vichi, M. (2013). Multiple stressors of ocean ecosystems in the 21st century : Projections with CMIP5  
3 models. *Biogeosciences*, 10(10), 6225-6245. <https://doi.org/10.5194/bg-10-6225-2013>

4 [Boucher, O., Servonnat, J., Albright, A. L., Aumont, O., Balkanski, Y., Bastrikov, V., Bekki, S., Bonnet, R., Bony, S.,  
5 Bopp, L., Braconnot, P., Brockmann, P., Cadule, P., Caubel, A., Cheruy, F., Codron, F., Cozic, A., Cugnet, D., D'Andrea,  
6 F., ... Vuichard, N. \(2020\). Presentation and Evaluation of the IPSL-CM6A-LR Climate Model. \*Journal of Advances in  
7 Modeling Earth Systems\*, 12\(7\), e2019MS002010. <https://doi.org/10.1029/2019MS002010>](#)

8 Browning, T. J., & Moore, C. M. (2023). Global analysis of ocean phytoplankton nutrient limitation reveals high prevalence  
9 of co-limitation. *Nature Communications*, 14(1), 5014. <https://doi.org/10.1038/s41467-023-40774-0>

10 [Christian, J. R., Denman, K. L., Hayashida, H., Holdsworth, A. M., Lee, W. G., Riche, O. G. J., Shao, A. E., Steiner, N.,  
11 & Swart, N. C. \(2022\). Ocean biogeochemistry in the Canadian Earth System Model version 5.0.3 : CanESM5 and  
12 CanESM5-CanOE. \*Geoscientific Model Development\*, 15\(11\), 4393-4424. <https://doi.org/10.5194/gmd-15-4393-2022>](#)

13 [Danabasoglu, G. \(2019\). NCAR CESM2-WACCM model output prepared for CMIP6 ScenarioMIP ssp245 \[Jeu de  
14 données\]. World Data Center for Climate \(WDCC\) at DKRZ. \[https://www.wdc-climate.de/ui/entry?acronym=C6\\\_4631838\]\(https://www.wdc-climate.de/ui/entry?acronym=C6\_4631838\)](#)

15 [Danabasoglu, G., Lamarque, J.-F., Bacmeister, J., Bailey, D. A., DuVivier, A. K., Edwards, J., Emmons, L. K., Fasullo, J.,  
16 Garcia, R., Gettelman, A., Hannay, C., Holland, M. M., Large, W. G., Lauritzen, P. H., Lawrence, D. M., Lenaerts, J. T.  
17 M., Lindsay, K., Lipscomb, W. H., Mills, M. J., ... Strand, W. G. \(2020\). The Community Earth System Model Version 2  
18 \(CESM2\). \*Journal of Advances in Modeling Earth Systems\*, 12\(2\), e2019MS001916.  
19 <https://doi.org/10.1029/2019MS001916>](#)

20 Doney, S. C. (2006). Phytoplankton in a warmer world. *Nature*, 444, 695-696.

21 Dunne, J. P., Horowitz, L. W., Adcroft, A. J., Ginoux, P., Held, I. M., John, J. G., Krasting, J. P., Malyshev, S., Naik, V.,  
22 Paulot, F., Shevliakova, E., Stock, C. A., Zadeh, N., Balaji, V., Blanton, C., Dunne, K. A., Dupuis, C., Durachta, J., Dussin,  
23 R., ... Zhao, M. (2020). The GFDL Earth System Model Version 4.1 (GFDL-ESM 4.1): Overall Coupled Model  
24 Description and Simulation Characteristics. *Journal of Advances in Modeling Earth Systems*, 12(11), e2019MS002015.  
25 <https://doi.org/10.1029/2019MS002015>

26 Embury, O. (2024). *ESA Sea Surface Temperature Climate Change Initiative (SST\_cci) : Climatology product, version 3.0*  
27 (NERC EDS Centre for Environmental Data Analysis) [Jeu de données].  
28 <https://doi.org/10.5285/62800d3d2227449085b430b503d36b01>

29 Eyring, V., Bony, S., Meehl, G. A., Senior, C. A., Stevens, B., Stouffer, R. J., & Taylor, K. E. (2016). Overview of the  
30 Coupled Model Intercomparison Project Phase 6 (CMIP6) experimental design and organization. *Geoscientific Model  
31 Development*, 9(5), 1937-1958. <https://doi.org/10.5194/gmd-9-1937-2016>

32 Fogli, P. G., & Iovino, D. (2014). *CMCC-CESM-NEMO : Toward the New CMCC Earth System Model* (SSRN Scholarly  
33 Paper N° 2603176). Social Science Research Network. <https://doi.org/10.2139/ssrn.2603176>

34 Fu, W., Randerson, J. T., & Moore, J. K. (2016). Climate change impacts on net primary production (NPP) and export  
35 production (EP) regulated by increasing stratification and phytoplankton community structure in the CMIP5 models.  
36 *Biogeosciences*, 13(18), 5151-5170. <https://doi.org/10.5194/bg-13-5151-2016>

a supprimé: Dufresne, J.-L., Foujols, M.-A., Denvil, S., Caubel, A., Marti, O., Aumont, O., Balkanski, Y., Bekki, S., Bellenger, H., Benshila, R., Bony, S., Bopp, L., Braconnot, P., Brockmann, P., Cadule, P., Cheruy, F., Codron, F., Cozic, A., Cugnet, D., ... Vuichard, N. (2013). Climate change projections using the IPSL-CM5 Earth System Model : From CMIP3 to CMIP5. *Climate Dynamics*, 40(9), 2123-2165. <https://doi.org/10.1007/s00382-012-1636-1>

a supprimé: G.,

a supprimé: Stouffer, R. J., Krasting, J. P., Malyshev, S. L., Milly, P. C. D., Sentman, L. T., Adcroft, A. J., Cooke, W

a supprimé: A., Griffies, S. M., Hallberg

a supprimé: W., Harrison, M. J., Levy, H., Wittenberg, A. T., Phillips, P. J., & Zadeh, N. (2013). GFDL's ESM2 Global

a supprimé: Climate-Carbon Earth System Models. Part II : Carbon System Formulation and Baseline

a supprimé: \*

a supprimé: *Climate*, 26(7), 2247-2267.

a supprimé: 1175/JCLI-D-12-00150.1

a supprimé: No.

a supprimé: .

1 Garcia, H. E., Boyer, T. P., Baranova, O. K., Locarnini, R. A., Mishonov, A. V., Grodsky, A., Paver, C. R., Weathers, K.  
2 W., Smolyar, I. V., Reagan, J. R., Seidov, D., & Zveng, M. M. (2019). *World Ocean Atlas 2018 : Product Documentation*.  
3 NOAA National Centers for Environmental Information.

4 [Gibson, G., Weijer, W., Jeffery, N., & Wang, S. \(2020\). Relative Impact of Sea Ice and Temperature Changes on Arctic  
5 Marine Production. \*Journal of Geophysical Research: Biogeosciences\*, 125\(7\), e2019JG005343.  
6 <https://doi.org/10.1029/2019JG005343>](#)

7 Grebmeier, J. M., Moore, S. E., Overland, J. E., Frey, K. E., & Gradinger, R. (2010). Biological Response to Recent Pacific  
8 Arctic Sea Ice Retreats. *Eos, Transactions American Geophysical Union*, 91(18), 161-162.  
9 <https://doi.org/10.1029/2010EO180001>

10 Gregg, W. W., & Rousseaux, C. S. (2019). Global ocean primary production trends in the modern ocean color satellite  
11 record (1998–2015). *Environmental Research Letters*, 14(12), 124011. <https://doi.org/10.1088/1748-9326/ab4667>

12 Hahn, L. C., Armour, K. C., Zelinka, M. D., Bitz, C. M., & Donohoe, A. (2021). Contributions to Polar Amplification in  
13 CMIP5 and CMIP6 Models. *Frontiers in Earth Science*, 9. <https://doi.org/10.3389/feart.2021.710036>

14 [Hajima, T., Watanabe, M., Yamamoto, A., Tatebe, H., Noguchi, M. A., Abe, M., Ohgaito, R., Ito, A., Yamazaki, D.,  
15 Okajima, H., Ito, A., Takata, K., Ogochi, K., Watanabe, S., & Kawamiya, M. \(2020\). Development of the MIROC-ES2L  
16 Earth system model and the evaluation of biogeochemical processes and feedbacks. \*Geoscientific Model Development\*,  
17 13\(5\), 2197-2244. <https://doi.org/10.5194/gmd-13-2197-2020>](#)

18 Haug, T., Bogstad, B., Chierici, M., Gjosæter, H., Hallfredsson, E., Høines, Å., Hoel, A. H., Ingvaldsen, R., Jørgensen, L.,  
19 Knutsen, T., Loeng, H., Naustvoll, L., Røttingen, I., & Sunnanå, K. (2017). Future harvest of living resources in the Arctic  
20 Ocean north of the Nordic and Barents Seas : A review of possibilities and constraints. *Fisheries Research*, 188, 38-57.  
21 <https://doi.org/10.1016/j.fishres.2016.12.002>

22 Hegseth, E. N., & Sundfjord, A. (2008). Intrusion and blooming of Atlantic phytoplankton species in the high Arctic.  
23 *Journal of Marine Systems*, 74(1), 108-119. <https://doi.org/10.1016/j.jmarsys.2007.11.011>

24 [Kwiatkowski, L., Torres, O., Bopp, L., Aumont, O., Chamberlain, M., Christian, J. R., Dunne, J. P., Gehlen, M., Ilyina, T.,  
25 John, J. G., Lenton, A., Li, H., Lovenduski, N. S., Orr, J. C., Palmieri, J., Santana-Falcón, Y., Schwinger, J., Séférian, R.,  
26 Stock, C. A., ... Ziehn, T. \(2020\). Twenty-first century ocean warming, acidification, deoxygenation, and upper-ocean  
27 nutrient and primary production decline from CMIP6 model projections. \*Biogeosciences\*, 17\(13\), 3439-3470.  
28 <https://doi.org/10.5194/bg-17-3439-2020>](#)

29 Lannuzel, D., Tedesco, L., van Leeuwe, M., Campbell, K., Flores, H., Delille, B., Miller, L., Stefels, J., Assmy, P.,  
30 Bowman, J., Brown, K., Castellani, G., Chierici, M., Crabeck, O., Damm, E., Else, B., Fransson, A., Fripiat, F., Geilfus,  
31 N.-X., ... Wongpan, P. (2020). The future of Arctic sea-ice biogeochemistry and ice-associated ecosystems. *Nature Climate  
32 Change*, 10(11), 983-992. <https://doi.org/10.1038/s41558-020-00940-4>

33 Laufkötter, C., Vogt, M., Gruber, N., Aita-Noguchi, M., Aumont, O., Bopp, L., Buitenhuis, E., Doney, S. C., Dunne, J.,  
34 Hashioka, T., Hauck, J., Hirata, T., John, J., Le Quéré, C., Lima, I. D., Nakano, H., Seferian, R., Totterdell, I., Vichi, M.,  
35 & Völker, C. (2015). Drivers and uncertainties of future global marine primary production in marine ecosystem models.  
36 *Biogeosciences*, 12(23), 6955-6984. <https://doi.org/10.5194/bg-12-6955-2015>

a supprimé: Ilyina, T., Six, K. D., Segsneider, J., Maier-Reimer, E., Li, H., & Núñez-Riboni, I. (2013). Global ocean biogeochemistry model HAMOCC : Model architecture and performance as component of the MPI-Earth system model in different CMIP5 experimental realizations. *Journal of Advances in Modeling Earth Systems*, 5(2), Article 2. <https://doi.org/10.1029/2012MS000178>

1 Lebrun, M., Vancoppenolle, M., Madec, G., Babin, M., Becu, G., Lourenço, A., Nomura, D., Vivier, F., & Delille, B.  
2 (2023). Light Under Arctic Sea Ice in Observations and Earth System Models. *Journal of Geophysical Research: Oceans*,  
3 *128*(3), e2021JC018161. <https://doi.org/10.1029/2021JC018161>

4 Lebrun, M., Vancoppenolle, M., Madec, G., & Massonnet, F. (2019). Arctic sea-ice-free season projected to extend into  
5 autumn. *The Cryosphere*, *13*(1), 79-96. <https://doi.org/10.5194/tc-13-79-2019>

6 Leu, E., Søreide, J. E., Hessen, D. O., Falk-Petersen, S., & Berge, J. (2011). Consequences of changing sea-ice cover for  
7 primary and secondary producers in the European Arctic shelf seas: Timing, quantity, and quality. *Progress in*  
8 *Oceanography*, *Arctic Marine Ecosystems in an Era of Rapid Climate Change*, *90*(1), 18-32.  
9 <https://doi.org/10.1016/j.pocean.2011.02.004>

10 Lewis, K. M., van Dijken, G. L., & Arrigo, K. R. (2020). Changes in phytoplankton concentration now drive increased  
11 Arctic Ocean primary production. *Science*, *369*(6500), 198-202. <https://doi.org/10.1126/science.aay8380>

12 Malik, I. H., & Ford, J. D. (2025). Understanding the Impacts of Arctic Climate Change Through the Lens of Political  
13 Ecology. *WIREs Climate Change*, *16*(1), e927. <https://doi.org/10.1002/wcc.927>

14 Manizza, M., Carroll, D., Menemenlis, D., Zhang, H., & Miller, C. E. (2023). Modeling the Recent Changes of  
15 Phytoplankton Blooms Dynamics in the Arctic Ocean. *Journal of Geophysical Research: Oceans*, *128*(6), e2022JC019152.  
16 <https://doi.org/10.1029/2022JC019152>

17 Marinov, I., Doney, S. C., & Lima, I. D. (2010). Response of ocean phytoplankton community structure to climate change  
18 over the 21st century: Partitioning the effects of nutrients, temperature and light. *Biogeosciences*, *7*(12), 3941-3959.  
19 <https://doi.org/10.5194/bg-7-3941-2010>

20 [Mauritsen, T., Bader, J., Becker, T., Behrens, J., Bittner, M., Brokopf, R., Brovkin, V., Claussen, M., Crueger, T., Esch,](#)  
21 [M., Fast, I., Fiedler, S., Fläschner, D., Gayler, V., Giorgetta, M., Goll, D. S., Haak, H., Hagemann, S., Hedemann, C., ...](#)  
22 [Roeckner, E. \(2019\). Developments in the MPI-M Earth System Model version 1.2 \(MPI-ESM1.2\) and Its Response to](#)  
23 [Increasing CO2. Journal of Advances in Modeling Earth Systems, 11\(4\), 998-1038.](#)  
24 <https://doi.org/10.1029/2018MS001400>

25 McCrystall, M. R., Stroeve, J., Serreze, M., Forbes, B. C., & Screen, J. A. (2021). New climate models reveal faster and  
26 larger increases in Arctic precipitation than previously projected. *Nature Communications*, *12*(1), 6765.  
27 <https://doi.org/10.1038/s41467-021-27031-y>

28 Meinshausen, M., Nicholls, Z. R. J., Lewis, J., Gidden, M. J., Vogel, E., Freund, M., Beyerle, U., Gessner, C., Nauels, A.,  
29 Bauer, N., Canadell, J. G., Daniel, J. S., John, A., Krummel, P. B., Luderer, G., Meinshausen, N., Montzka, S. A., Rayner,  
30 P. J., Reimann, S., ... Wang, R. H. J. (2020). The shared socio-economic pathway (SSP) greenhouse gas concentrations  
31 and their extensions to 2500. *Geoscientific Model Development*, *13*(8), 3571-3605. [https://doi.org/10.5194/gmd-13-3571-](https://doi.org/10.5194/gmd-13-3571-2020)  
32 [2020](https://doi.org/10.5194/gmd-13-3571-2020)

33 Moore, J. K., Lindsay, K., Doney, S. C., Long, M. C., & Misumi, K. (2013). *Marine Ecosystem Dynamics and*  
34 *Biogeochemical Cycling in the Community Earth System Model [CESM1(BGC)] : Comparison of the 1990s with the 2090s*  
35 *under the RCP4.5 and RCP8.5 Scenarios*. <https://doi.org/10.1175/JCLI-D-12-00566.1>

1 Mudryk, L. R., Dawson, J., Howell, S. E. L., Derksen, C., Zagon, T. A., & Brady, M. (2021). Impact of 1, 2 and 4 °C of  
2 global warming on ship navigation in the Canadian Arctic. *Nature Climate Change*, 11(8), 673-679.  
3 <https://doi.org/10.1038/s41558-021-01087-6>

4 Nakamura, Y., & Oka, A. (2019). CMIP5 model analysis of future changes in ocean net primary production focusing on  
5 differences among individual oceans and models. *Journal of Oceanography*, 75(5), 441-462.  
6 <https://doi.org/10.1007/s10872-019-00513-w>

7 Neukermans, G., Oziel, L., & Babin, M. (2018). Increased intrusion of warming Atlantic water leads to rapid expansion of  
8 temperate phytoplankton in the Arctic. *Global Change Biology*, 24(6), 2545-2553. <https://doi.org/10.1111/gcb.14075>

9 Notz, D., & Community, S. (2020). Arctic Sea Ice in CMIP6. *Geophysical Research Letters*, 47(10), e2019GL086749.  
10 <https://doi.org/10.1029/2019GL086749>

11 OSI SAF. (2022). *Global Sea Ice Concentration Climate Data Record v3.0—Multimission* (EUMETSAT SAF on Ocean  
12 and Sea Ice) [Jeu de données]. [https://doi.org/10.15770/EUM\\_SAF\\_OSI\\_0013](https://doi.org/10.15770/EUM_SAF_OSI_0013)

13 Oziel, L., Gürses, Ö., Torres-Valdés, S., Hoppe, C. J. M., Rost, B., Karakuş, O., Danek, C., Koch, B. P., Nissen, C.,  
14 Koldunov, N., Wang, Q., Völker, C., Iversen, M., Juhls, B., & Hauck, J. (2025). Climate change and terrigenous inputs  
15 decrease the efficiency of the future Arctic Ocean's biological carbon pump. *Nature Climate Change*, 15(2), 171-179.  
16 <https://doi.org/10.1038/s41558-024-02233-6>

17 Pabi, S., van Dijken, G. L., & Arrigo, K. R. (2008). Primary production in the Arctic Ocean, 1998–2006. *Journal of*  
18 *Geophysical Research: Oceans*, 113(C8). <https://doi.org/10.1029/2007JC004578>

19 Popova, E. E., Yool, A., Coward, A. C., Aksenov, Y. K., Alderson, S. G., de Cuevas, B. A., & Anderson, T. R. (2010).  
20 Control of primary production in the Arctic by nutrients and light : Insights from a high resolution ocean general circulation  
21 model. *Biogeosciences*, 7(11), 3569-3591. <https://doi.org/10.5194/bg-7-3569-2010>

22 ~~Randelhoff, A., Holding, J., Janout, M., Sejr, M. K., Babin, M., Tremblay, J.-É., & Alkire, M. B. (2020). Pan-Arctic Ocean~~  
23 ~~Primary Production Constrained by Turbulent Nitrate Fluxes. *Frontiers in Marine Science*, 7.~~  
24 ~~<https://doi.org/10.3389/fmars.2020.00150>~~

25 Rantanen, M., Karpechko, A. Y., Lipponen, A., Nordling, K., Hyvärinen, O., Ruosteenoja, K., Vihma, T., & Laaksonen,  
26 A. (2022). The Arctic has warmed nearly four times faster than the globe since 1979. *Communications Earth &*  
27 *Environment*, 3(1), 168. <https://doi.org/10.1038/s43247-022-00498-3>

28 ~~Rohr, T., Richardson, A. J., Lenton, A., Chamberlain, M. A., & Shadwick, E. H. (2023). Zooplankton grazing is the largest~~  
29 ~~source of uncertainty for marine carbon cycling in CMIP6 models. *Communications Earth & Environment*, 4(1), 212.~~  
30 ~~<https://doi.org/10.1038/s43247-023-00871-w>~~

31 Sarmiento, J. L. (2013). Ocean Biogeochemical Dynamics. In *Ocean Biogeochemical Dynamics*. Princeton University  
32 Press. <https://www.degruyterbrill.com/document/doi/10.1515/9781400849079/html>

33 Sarthou, G., Timmermans, K. R., Blain, S., & Tréguer, P. (2005). Growth physiology and fate of diatoms in the ocean : A  
34 review. *Journal of Sea Research*, *Iron Resources and Oceanic Nutrients - Advancement of Global Environmental*  
35 *Simulations*, 53(1), 25-42. <https://doi.org/10.1016/j.seares.2004.01.007>

a supprimé: No.

a supprimé: Popova, E. E., Yool, A., Coward, A. C., Dupont, F., Deal, C., Elliott, S., Hunke, E., Jin, M., Steele, M., & Zhang, J. (2012). What controls primary production in the Arctic Ocean? Results from an intercomparison of five general circulation models with biogeochemistry. *Journal of Geophysical Research: Oceans*, 117(C8). <https://doi.org/10.1029/2011JC007112>

a supprimé: Riahi, K., Rao, S., Krey, V., Cho, C., Chirkov, V., Fischer, G., Kindermann, G., Nakicenovic, N., & Rafaj, P. (2011). RCP 8.5—A scenario of comparatively high greenhouse gas emissions. *Climatic Change*, 109(1), 33. <https://doi.org/10.1007/s10584-011-0149-y>

1 Schulzweida, U. (2023). *CDO User Guide*. <https://doi.org/10.5281/zenodo.10020800>

2 [Séférian, R., Nabat, P., Michou, M., Saint-Martin, D., Voldoire, A., Colin, J., Decharme, B., Delire, C., Berthet, S.,](#)  
3 [Chevallier, M., Sénési, S., Franchisteguy, L., Vial, J., Mallet, M., Joetzjer, E., Geoffroy, O., Guérémy, J.-F., Moine, M.-P.,](#)  
4 [Msadek, R., ... Madec, G. \(2019\). Evaluation of CNRM Earth System Model, CNRM-ESM2-1 : Role of Earth System](#)  
5 [Processes in Present-Day and Future Climate. \*Journal of Advances in Modeling Earth Systems\*, 11\(12\), 4182-4227.](#)  
6 <https://doi.org/10.1029/2019MS001791>

7 [Sellar, A. A., Jones, C. G., Mulcahy, J. P., Tang, Y., Yool, A., Wiltshire, A., O'Connor, F. M., Stringer, M., Hill, R.,](#)  
8 [Palmieri, J., Woodward, S., de Mora, L., Kuhlbrodt, T., Rumbold, S. T., Kelley, D. I., Ellis, R., Johnson, C. E., Walton, J.,](#)  
9 [Abraham, N. L., ... Zerroukat, M. \(2019\). UKESM1 : Description and Evaluation of the U.K. Earth System Model. \*Journal\*](#)  
10 [of Advances in Modeling Earth Systems](#), 11(12), 4513-4558. <https://doi.org/10.1029/2019MS001739>

11 Shu, Q., Qiao, F., Song, Z., Zhao, J., & Li, X. (2018). Projected Freshening of the Arctic Ocean in the 21st Century. *Journal*  
12 *of Geophysical Research: Oceans*, 123(12), 9232-9244. <https://doi.org/10.1029/2018JC014036>

13 [Steiner, N. S., Sou, T., Deal, C., Jackson, J. M., Jin, M., Popova, E., Williams, W., & Yool, A. \(2016\). The future of the](#)  
14 [subsurface chlorophyll-a maximum in the Canada Basin—A model intercomparison. \*Journal of Geophysical Research:\*](#)  
15 [Oceans](#), 121(1), 387-409. <https://doi.org/10.1002/2015JC011232>

16 [Swart, N. C., Cole, J. N. S., Kharin, V. V., Lazare, M., Scinocca, J. F., Gillett, N. P., Anstey, J., Arora, V., Christian, J. R.,](#)  
17 [Hanna, S., Jiao, Y., Lee, W. G., Majaess, F., Saenko, O. A., Seiler, C., Seinen, C., Shao, A., Sigmond, M., Solheim, L., ...](#)  
18 [Winter, B. \(2019\). The Canadian Earth System Model version 5 \(CanESM5.0.3\). \*Geoscientific Model Development\*,](#)  
19 [12\(11\), 4823-4873. https://doi.org/10.5194/gmd-12-4823-2019](#)

20 Tagliabue, A., Kwiatkowski, L., Bopp, L., Butenschön, M., Cheung, W., Lengaigne, M., & Vialard, J. (2021). Persistent  
21 Uncertainties in Ocean Net Primary Production Climate Change Projections at Regional Scales Raise Challenges for  
22 Assessing Impacts on Ecosystem Services. *Frontiers in Climate*, 3.  
23 <https://www.frontiersin.org/articles/10.3389/fclim.2021.738224>

24 Taylor, K. E., Stouffer, R. J., & Meehl, G. A. (2012). An Overview of CMIP5 and the Experiment Design. *Bulletin of the*  
25 *American Meteorological Society*, 93(4). <https://journals.ametsoc.org/view/journals/bams/93/4/bams-d-11-00094.1.xml>

26 Terhaar, J., Lauerwald, R., Regnier, P., Gruber, N., & Bopp, L. (2021). Around one third of current Arctic Ocean primary  
27 production sustained by rivers and coastal erosion. *Nature Communications*, 12(1), Article 1.  
28 <https://doi.org/10.1038/s41467-020-20470-z>

29 [Timmermans, M.-L., & Marshall, J. \(2020\). Understanding Arctic Ocean Circulation : A Review of Ocean Dynamics in a](#)  
30 [Changing Climate. \*Journal of Geophysical Research: Oceans\*, 125\(4\), e2018JC014378.](#)  
31 <https://doi.org/10.1029/2018JC014378>

32 [Tjiputra, J. F., Schwinger, J., Bentsen, M., Morée, A. L., Gao, S., Bethke, I., Heinze, C., Goris, N., Gupta, A., He, Y.-C.,](#)  
33 [Olivié, D., Seland, Ø., & Schulz, M. \(2020\). Ocean biogeochemistry in the Norwegian Earth System Model version 2](#)  
34 [\(NorESM2\). \*Geoscientific Model Development\*, 13\(5\), 2393-2431. https://doi.org/10.5194/gmd-13-2393-2020](#)

**a supprimé:** The HadGEM2 Development Team: G. M. Martin, Bellouin, N., Collins, W. J., Culverwell, I. D., Halloran, P. R., Hardiman, S. C., Hinton, T. J., Jones, C. D., McDonald, R. E., McLaren, A. J., O'Connor, F. M., Roberts, M. J., Rodriguez, J. M., Woodward, S., Best, M. J., Brooks, M. E., Brown, A. R., Butchart, N., Dearden, C., ... Wiltshire, A. (2011). The HadGEM2 family of Met Office Unified Model climate configurations. *Geoscientific Model Development*, 4(3), 723-757. <https://doi.org/10.5194/gmd-4-723-2011>

1 Tremblay, J.-E., & Gagnon, J. (2009). The effects of irradiance and nutrient supply on the productivity of Arctic waters :  
 2 A perspective on climate change. In *Influence of Climate Change on the Changing Arctic and Sub-Arctic Conditions* (Vol.  
 3 73–93, p. 73-93). [https://doi.org/10.1007/978-1-4020-9460-6\\_7](https://doi.org/10.1007/978-1-4020-9460-6_7)

4 Vancoppenolle, M., Bopp, L., Madec, G., Dunne, J., Ilyina, T., Halloran, P. R., & Steiner, N. (2013). Future Arctic Ocean  
 5 primary productivity from CMIP5 simulations : Uncertain outcome, but consistent mechanisms. *Global Biogeochemical*  
 6 *Cycles*, 27(3), 605-619. <https://doi.org/10.1002/gbc.20055>

7 Vincent, W. F., & Laybourn-Parry, J. (2008). *Polar Lakes and Rivers : Limnology of Arctic and Antarctic Aquatic*  
 8 *Ecosystems*. Oxford University Press.

9 Ward, B. A., Dutkiewicz, S., Jahn, O., & Follows, M. J. (2012). A size-structured food-web model for the global ocean.  
 10 *Limnology and Oceanography*, 57(6), 1877-1891. <https://doi.org/10.4319/lo.2012.57.6.1877>

11 Wassmann, P. (2011). Arctic marine ecosystems in an era of rapid climate change. *Progress in Oceanography*, *Arctic*  
 12 *Marine Ecosystems in an Era of Rapid Climate Change*, 90(1), 1-17. <https://doi.org/10.1016/j.pocean.2011.02.002>

13 Wassmann, P., Reigstad, M., Haug, T., Rudels, B., Carroll, M. L., Hop, H., Gabrielsen, G. W., Falk-Petersen, S.,  
 14 Denisenko, S. G., Arashkevich, E., Slagstad, D., & Pavlova, O. (2006). Food webs and carbon flux in the Barents Sea.  
 15 *Progress in Oceanography*, *Structure and function of contemporary food webs on Arctic shelves: a pan-Arctic comparison*,  
 16 71(2), 232-287. <https://doi.org/10.1016/j.pocean.2006.10.003>

17 Weijer, W., Cheng, W., Garuba, O. A., Hu, A., & Nadiga, B. T. (2020). CMIP6 Models Predict Significant 21st Century  
 18 Decline of the Atlantic Meridional Overturning Circulation. *Geophysical Research Letters*, 47(12), e2019GL086075.  
 19 <https://doi.org/10.1029/2019GL086075>

20 Yukimoto, S., Kawai, H., Koshiro, T., Oshima, N., Yoshida, K., Urakawa, S., Tsujino, H., Deushi, M., Tanaka, T., Hosaka,  
 21 M., Yabu, S., Yoshimura, H., Shindo, E., Mizuta, R., Obata, A., Adachi, Y., & Ishii, M. (2019). The Meteorological  
 22 Research Institute Earth System Model Version 2.0. MRI-ESM2.0 : Description and Basic Evaluation of the Physical  
 23 Component. *気象集誌 第2輯*, 97(5), 931-965. <https://doi.org/10.2151/jmsj.2019-051>

24 Zelinka, M. D., Myers, T. A., McCoy, D. T., Po-Chedley, S., Caldwell, P. M., Ceppi, P., Klein, S. A., & Taylor, K. E.  
 25 (2020). Causes of Higher Climate Sensitivity in CMIP6 Models. *Geophysical Research Letters*, 47(1), e2019GL085782.  
 26 <https://doi.org/10.1029/2019GL085782>

a supprimé: Watanabe, S., Hajima, T., Sudo, K., Nagashima, T., Takemura, T., Okajima, H., Nozawa, T., Kawase, H., Abe, M., Yokohata, T., Ise, T., Sato, H., Kato, E., Takata, K., Emori, S., & Kawamiya, M. (2011). MIROC-ESM 2010 : Model description and basic results of CMIP5-20c3m experiments. *Geoscientific Model Development*, 4(4), 845-872. <https://doi.org/10.5194/gmd-4-845-2011>

**Page 9 : [1] a supprimé**                      **lena.cbcb12010@gmail.com**                      **09/06/2026 10:49:00**



**Page 12 : [2] a supprimé**                      **lena.cbcb12010@gmail.com**                      **09/06/2026 10:49:00**



**Page 21 : [3] a supprimé**                      **lena.cbcb12010@gmail.com**                      **09/06/2026 10:49:00**



**Page 27 : [4] a supprimé**                      **lena.cbcb12010@gmail.com**                      **09/06/2026 10:49:00**

